This is a previous version of the article published in Ecotoxicology and Environmental Safety. 2020, 192: 110272. doi:10.1016/j.ecoenv.2020.110272

Photodecomposition Properties of Brominated Flame Retardants (BFRs)

Anam Saeed[a], Mohammednoor Altarawneh[a,*], Kamal Siddique[a], Juan A. Conesa[b], Nuria Ortuño[b] and Bogdan Z. Dlugogorski[a]

[a]School of Engineering and Information Technology, Murdoch University

90 South Street, Murdoch, WA 6150, Australia

[b]Department of Chemical Engineering, University of Alicante, P.O. Box 99, Alicante, Spain

[*]Corresponding author:

Phone: +61 8 9360 7507, Email: M.Altarawneh@murdoch.edu.au

Abstract

This study investigates the geometric and electronic properties of selected BFRs in their ground (S_0) and first singlet excited (S_1) states deploying methods of the density functional theory (DFT) and the time-dependent density functional theory (TDDFT). We estimate the effect of the $S_0 \rightarrow S_1$ transition on the elongations of the C-Br bond, identify the frontier molecular orbitals involved in the excitation process and compute partial atomic charges for the most photoreactive bromine atoms. The bromine atom attached to an *ortho* position in HBB (with regard to C-C bond; 2,2′,4,4′,6,6′-hexabromobiphenyl), TBBA (with respect to the hydroxyl group; 2,2′,6,6′-tetrabromobisphenol A), HBDE and BTBPE (in reference to C-O linkage; 2,2′,4,4′,6,6′-hexabromodiphenylether and 1,2-bis(2,4,6-tribromophenoxy)ethane, respectively) bears the highest positive atomic charge. This suggests that, these positions undergo reductive debromination reactions to produce lower brominated molecules. Debromination reactions ensue primarily in the aromatic compounds substituted with the highest number of bromine atoms owing to the largest stretching of the C-Br bond in the first excited state. The analysis of the frontier molecular orbitals indicates that, excitations of BFRs proceed via $\pi \rightarrow \pi^*$, or $\pi \rightarrow \sigma^*$ or $n \rightarrow \sigma^*$ electronic transitions. The orbital analysis reveals that, the HOMO-LUMO energy gap ($E^{H\text{-}L}$) for all investigated bromine-substituted aromatic molecules falls lower (1.85 – 4.91 eV) than for their non-brominated analogues (3.39 – 8.07 eV), in both aqueous and gaseous media. The excitation energies correlate with the $E^{H\text{-}L}$ values. The excitation energies and $E^{H\text{-}L}$ values display a linear negative correlation with the number of bromine atoms attached to the molecule. Spectral analysis of the gaseous-phase systems reveals that, the highly brominated aromatics endure lower excitation energies and exhibit red shifts of their absorption bands in comparison to their lower brominated congeners. We attained a satisfactory agreement between the experimentally measured absorption peak (λ_{max})

and the theoretically predicted oscillator strength (λ_{max}) for the UV-Vis spectra. This study further confirms that, halogenated aromatics only absorb light in the UV spectral region and that effective photodegradation of these pollutants requires the presence of photocatalysts.

Key words

Brominated flame retardants (BFRs); Time dependent density functional theory (TDDFT), Photodegradation, Geometric and electronic properties, Excited states.

1. Introduction

Brominated flame retardants (BFRs) comprise bromine-bearing hydrocarbons commonly added to the polymeric constituents in consumer products to enhance their fire retardancy. In light of their substantial deployment over the past two decades, BFRs have accumulated in various environmental compartments spaning sewage sludge, sediments (Sellström et al., 1999; Morris et al., 2004), air samples and water bodies (Covaci et al., 2003; Eljarrat et al., 2005; Möller et al., 2011). While the historically-employed BFRs persist in the environment, recent investigations have revealed alarming concentrations of the so-called novel BFRs (Ali et al., 2011a,b; Covaci et al., 2011; de Wit, 2002; Eriksson et al., 2001; Fromme et al., 2014).

The bioaccumulative and persistent nature of BFRs renders them as one of the main themes of research among environmental chemists. High concentrations of certain BFRs are adequate to provoke toxic effects in humans and wildlife (Darnerud, 2003; Watanabe and Sakai, 2003). While BFRs can be toxic in their own right, the major environmental burden of BFRs rests on their structural functionality as direct building blocks for the generation of notorious polybrominated dibenzo-*p*-dioxins and dibenzofurans (PBDD/Fs) (Buser, 1986; Luijk and Govers, 1992; Sakai et al., 2001; Weber and Kuch, 2003). As the thermal treatment represents a mainstream strategy in recovery and disposal of materials laden with BFRs (i.e., plastics and electronic wastes), several studies have elucidated scenarios and pathways underpinning the transformation of BFRs into PBDD/Fs at elevated temperatures relevant to "waste-to-energy" applications (Altarawneh and Dlugogorski, 2013, 2014a,b, 2015). In addition to formation of PBDD/Fs, the thermal decomposition of BFRs generates a wide array of small brominated C_1-C_4 species as well as large macromolecules (Barontini and Cozzani, 2006; Barontini et al., 2004; Luda et al., 2002; Ortuño et al., 2014; Saeed et al., 2015, 2016a).

BFRs enter the environment via several routes, most notably, through direct diffusion from treated objects at room temperature (Choi et al., 2009; Stapleton et al., 2011) and from open burning and dumping of BFR-containing materials (Gullett et al., 2007; Eguchi et al., 2013; Tian et al., 2011). This makes it important to trace down the chemical transformation pathways of BFRs in the environment. While thermal processes decontaminate BFRs by destroying their structures, pathways prevailing in the environment are fundamentally distinct.

Photolysis constitute the primary environmental route for the chemical transformation of BFRs. Most relevant experimental investigations have focused on the photo-induced decay of polybrominated diphenyl ethers (PBDEs). Söderström et al. investigated photolysis of decaBDE in different environmental matrices (Söderström et al., 2004). Various sunlight conditions induce the formation of lower brominated congeners of diphenylethers, especially the lower isomers of PBDEs and PBDFs. The medium of reaction (i.e., solid, sediment and sand) exhibits little influence on the debromination process, however, it significantly affects the temporal scale of the reaction. Few studies (Eriksson et al., 2004; Watanabe and Tatsukawa, 2008; Norris et al., 1973) consistently reported the debromination during the course of photolysis of PBDEs. Eriksson et al. (2004) observed different isomers of PBDEs exhibiting distinct photolytic decay rates. Similarly, experiments of Otha et al. (2001) established that, different sources of light (sunlight versus UV-lamps) produce diverse patterns of debrominated products.

Theoretical calculations based on the time-dependent density functional theory (TDDFT) formalism elucidated structures and electronic properties of various BFRs at their first excited states, as function of their photoreactivity (Luo et al., 2015; Sun et al., 2013; Suh et al., 2009;

Wang et al., 2012). These investigations assessed (i) the transformation of brominated moieties in their singlet or triplet excited states and (ii) the effect of the degree and pattern of bromination on the photodecomposition processes. Along this line of inquiry, in our recent theoretical contribution, we have computed properties of the complete series of bromophenols (BPhs) in their ground and first excited states (Saeed et al., 2016b). Our results articulate that, when brominated compounds become photoexcited, the rate of debromination follows the sequence of *ortho>meta>para* positions. Furthermore, congeners entailing a high degree of bromination demand lower excitation energies and photodecompose more readily than the lower brominated isomers. Thus, the reductive photodebromination depends on the pattern and degree of bromine substituents on the aromatic ring.

Brominated aromatic compounds, in general, absorb light in the UV region. Sufficient amount of captured electromagnetic energy triggers a facile homolytic fission of C-Br bond and provokes structural rearrangements, including cleavage of the ether bond. Mechanistically, the UV energy absorbed in a molecule prompts the appearance of two pathways (i) a large fraction of energy engenders electron transitions between π and π^* and between n and σ^* orbitals, (ii) whereas the remainder induces the rupture of the C-Br bonds (Joschek and Miller, 1966). In a nutshell, photoexcited BFRs undergo singlet or triplet excited state transitions that involve weakening of the aromatic C-Br bonds.

While daylight has no capacity to photodecompose neat BFRs, certain species in the aqueous medium can act as photocatalysts. A pioneering study by Sun et al. has demonstrated the role of carboxylate anions to mediate reductive debromination of PBDEs in visible light (Sun et al., 2103). The BFRs probably coexist with organic acids in the environment. For example, the

hydrophobic nature of BFRs facilitates their adsorption in the outer waxy surfaces of plants and even on human skin (Jaward et al., 2004; Mimmoa et al., 2011).

The reported reductive debromination of BFRs in the ambient environment has motivated us to study the properties of selected BFRs on the verge of their photodecomposition. To this end, the current contribution elucidates results of DFT and TDDFT calculations designed to evaluate the photodecomposition behaviour of the most commonly deployed BFRs as function of degree of bromination. Investigated BFRs include polybrominated biphenyls, polybrominated diphenylethers, polybrominated bisphenols, 1,2-bis(2,4,6-tribromophenoxy)ethane and bromocyclododecane. To study the effect of degree of bromination, we selected hexa, tetra and dibrominated congeners of biphenyls and diphenylethers that include 2,2′,4,4′,6,6′-hexabromobiphenyl (HBB), 2,2′,4,4′-tetrabromobiphenyl (TBB) and 4,4′-dibromobiphenyl (DBB), 2,2′,4,4′,6,6′-hexabromodiphenylether (HBDE), 2,2′,4,4′-tetrabromodiphenylether (TBDE) and 4,4′-dibromodiphenylether (DBDE), as well as congeners of brominated bisphenol, such as 2,2′,6,6′-tetrabromobisphenol A (TBBA), 2,2′,6-tribromobisphenol (TriBBA) and 2,2′-dibromobisphenol (DBBA). Likewise, we investigate congeners of 1,2-bis(2,4,6-tribromophenoxy)ethane, including 1,2-bis(2,4,6-tribromophenoxy)ethane (BTBPE) itself, 1,2-bis(2,4-dibromophenoxy)ethane (BDBPE) and 1,2-bis(4-bromophenoxy)ethane (BMDPE), and study brominated congeners of cyclododecane comprising 1,2,5,6,9,10-hexabromocyclododecane (HBCD), 1,2,5,6-tetrabromocyclododecane (TBCD) and 1,2-dibromocyclododecane (DBCD). We capture the effect of bromine loading on the electronic and structural properties by contrasting the results for brominated species with their non-brominated analogues. Investigated properties include energies of the lowest excited singlet states, oscillator strength, partial atomic charges and UV-Vis absorption spectra. We find it

particularly important to report the properties of the first excited states of the studied BFRs in aqueous phase, as Sun et al. (2013) discovered the decomposition of PBDEs by visible light in the presence of carboxylate anions. We also elucidate a relationship between the thermal stability and photoreactivity of selected molecules, by studying the difference in energy between frontier molecular orbitals and the electronic charges. This energy difference constitutes prominent molecular descriptors of stability and photoreactivity of BFRs. Finally, we report experimentally measured UV-Vis spectra for TBBA and bisphenol A to benchmark the results of our theoretical calculations for their accuracy.

2. Methods

2.1. Computational details

Electronic structure calculations for selected brominated and non-brominated molecules of the flame retardant in the ground and excited states were executed using Accelrys' DMol^3 (Delley, 2000) program. Geometry optimisation for all structures was performed using the DFT functional of GGA-PW91 (Perdew et al., 1992). The theoretical approach encompasses a double numerical basis set with *d* polarisation function (DND) (1998) with an orbital cut-off radius of 4.4 Å for numerical integration. The size of our numerical basis set is comparable to the Gaussian basis set of 6-31G*. Owing to the numerical optimisation, the DND basis set displays improved accuracy and holds small superposition errors than a size-equivalent Gaussian basis set (Delley, 1990).

We deployed a conductor-like screening model (COSMO) to include the solvation effects in geometry optimisation (Klamt and Schüürmann, 1993; Klamt, 1995). All aqueous phase calculations involve relative permittivity of water of 78.5. We study the excited states of considered molecules by implementing the TDDFT approach (geometric convergence set to 10^{-6} Ha) along with the adiabatic local exchange density functional approximation (ALDA) (Zangwill and Soven, 1980). The UV-Vis absorption spectra were simulated using TDDFT calculations for the ground and excited state both in gaseous and aqueous phases (Delley, 2010). Eq. 1 illustrates the electronic transition from the initial (*i*) to final (*f*) states in the absorption process (Yao and Lin, 2008; Zhu et al., 2009; Wang et al., 2009):

$$W_{i\to f}(\omega) = \frac{2\pi}{h^2}\left|\mu_{fi.}E_0(\omega)\right|^2 \sum_v \sum_{v'} P_{iv} \left|\left(\Theta_{fv'}\middle|\Theta_{iv}\right)\right|^2 D(\omega_{fv',iv} - \omega_{,}\gamma_{fv',iv}) \quad \text{[Eq. 1]}$$

Whereas, Eq. 2 expresses the UV-Vis absorption spectrum:

$$\alpha(\omega) = \frac{4\pi^2\omega}{3\hbar ca}|\mu_{fi}|^2 \sum_v \sum_{v'} P_{iv}\left|\left(\Theta_{fv'}\middle|\Theta_{iv}\right)\right|^2 D\left(\omega_{fv',iv} - \omega_{,}\gamma_{fv',iv}\right) \quad \text{[Eq. 2]}$$

In Eqs [1] and [2], μ_{fi} signifies the electronic transition dipole moment between the *i* and *f* states, E_0 denotes the amplitude of the vector for the incident sinusoidal electric field and P_{iv} stands for the Boltzmann distribution factor. The expression $\left|\left(\Theta_{fv'}\middle|\Theta_{iv}\right)\right|$ characterises the Frank-Condon factor and $D(\omega_{fv',iv} - \omega_{,}\gamma_{fv',iv})$ denotes the Lorentzian-shape function with a damping factor (γ). Furthermore, *v* and *v′* are the vibrational quantum numbers corresponding to the electronic states *i* and *f*, *c* stands for the speed of light and *a* expresses the solvation effect.

We examined the atomic charges for the most photoreactive bromine atoms in BFR compounds based on the Hirshfeld population analysis (Delley, 1990). Hirshfeld methods constitute the most accurate computational formalism for the determination of atomic charges (Fonseca et al., 2004). The calculations of the optical properties of both gaseous and aqueous phases in the ground and excited state involved the optimised ground state molecular structures (Zhao and Han, 2009).

2.2. Experimental

We selected TBBA and bisphenol A for the experimental measurement of UV-Vis spectra. TBBA sample exists as a white solid powder purchased from Sigma Aldrich, Australia. Novachem, Australia (representative of Cambridge Isotope Laboratories, LGC, AccuStandard and Cerilliant) supplied a standard solution of bisphenol A in methanol. We acquired hexane and methanol solvents of GC grade (purity > 99.9 %) for the preparation of TBBA and bisphenol A solutions, respectively, from Chem Supply, Australia. The UV-Vis spectra of both samples were recorded in the region of 190 nm – 800 nm on ultra violet-visible-near infrared spectrometer (Cary 5000 UV-Vis-NIR from Agilent Technologies) at 1 nm interval. The UV-Vis spectra of neat solvents served as the baseline corrections.

3. Results and Discussion

3.1 Optimised structures in ground and excited states of selected BFRs

Fig. 1 presents optimised geometries of the considered BFRs and their non-brominated counterparts, in the gaseous phase at the ground state (S_0), along with illustrative numbering of atoms and C-Br bond lengths (in Å). While HBCDs assume various energy-degenerate structural configurations, we elect to study properties of the δ isomer (Heeb et al., 2005). Table 1 lists prominent interatomic distances for C-Br bonds in configurations arising in the gaseous and aqueous phases, for the S_0 and the first excited state (S_1); refer to Fig. 1 for numbering of atoms. Contrasting the geometrical features in the S_0 and S_1 states provides valuable insight into trends governing the photodecomposition process as well as the effect of the degree of bromination on the photoreactivity of the title BFRs.

The structural parameters (particularly carbon-halogen bond lengths) of brominated compounds in the S_0 state differ from those in the S_1 state; both in the gaseous and aqueous phases. Upon excitation from the S_0 to the S_1 state, C-Br bonds elongate, especially those at *ortho* position (Alaee et al., 2003; Li et al., 2007), leading us to make the following remarks:

(i) For brominated biphenyls, we observe the most extended elongation of the C-Br bond at the *ortho* position with respect to the C-C bridge, i.e., 4.4 % and 5.7 % for HBB in gaseous and aqueous phases, respectively. Corresponding distances at the *meta* positions lengthened by 2.9 % for HBB and 3.6 % for DBB. Thus, the degree of elongation of C-Br bond for $S_0 \rightarrow S_1$ transitions follow the sequence of *ortho*>*meta* sites.

(ii) For PBDEs, the maximum lengthening of C-Br bond occurs at the *ortho* position with regard to the O-C bridge. For higher brominated congeners such as HBDE, the extent of C-Br bond elongation exceeds that for the lower brominated species

for the same position. For example, the *ortho* and *meta* C-Br bond elongations in HBDE amount to 6.1 % and 4.4 %, respectively. These percentages slightly overshoot the analogous values reported for DBDE at 5.3 % and 4.1 %, correspondingly. Moreover, the presence of solvent media like water does not alter the position of the most elongated C-Br bond. However, relative stretching (in %, in reference to equilibrium distances in the S_0 state) reduces slightly for PBDEs in the aqueous medium.

(iii) In brominated congeners of bisphenol A, one *ortho* C-Br bond (with respect to the hydroxyl group), presents significant elongation of 8.8 % and 9.0 % for TBBA and TriBBA, respectively. The C-Br bonds in the other *ortho* positions stretch by 2.9 % – 7.2 %, revealing the dependence of bond elongation on the position and degree of bromine substitution on the aromatic ring.

(iv) In BTBPE and BDBPE, the bromine substitution at the *ortho* position (with respect to the C-O linkage) results in 7.1 % and 4.5 % lengthening of the C-Br bond in the first excited state in the gaseous phase, in that order. The C-Br bond stretching for BTBPE, BDBPE and BMBPE molecules at the *meta* position fall below these values, amounting to 4.4 %, 4.0 % and 1.8 %, respectively.

(v) The C-Br bonds in non-aromatic HBCD experience stretching upon the $S_0 \rightarrow S_1$ transition, by 0.18 Å in gaseous and 0.17 Å in aqueous media. Our computed C-Br bond lengths in the gaseous S_0 state lie in the range of 2.023 – 2.044 Å and are in reasonable agreement with other theoretically computed C-Br bond lengths for gaseous systems (i.e., 1.991 – 2.020 Å) (Zhao et al., 2010).

(vi) The extent of elongation (as a percentage and an absolute value) of C-Br bonds displays inconsistent variations in gaseous and aqueous media. The extent of C-Br bond stretching in PBBs, PBDEs, BTBPEs and PBCDs in $S_0 \rightarrow S_1$ transitions in gaseous phase exceed that in aqueous medium. However, for $S_0 \rightarrow S_1$ shift, the percentage elongation of C-Br bonds in brominated congeners of bisphenol A in aqueous phase surpasses the analogous extensions in the gaseous phase. For example, the *ortho* C-Br (with respect to C-O linkage) in BTBPE in the gaseous phase elongates by 0.109 Å (5.6 %) in comparison with 0.074 Å (3.8 %) in the aqueous medium. However, in TriBBA, the *ortho* C-Br (with respect to O-H bridge) elongates by 0.157 Å (8.02 %) in aqueous phase; slightly higher than the analogous elongation in the gaseous phase, reported as 0.139 Å (7.2 %). Therefore, we deduce that, the relative tendency of debromination of BFRs in the gaseous vs aqueous medium rests on the structure of the BFRs.

(vii) No significant variation in the geometries appears when exciting the non-brominated species from the S_0 to the S_1 states in both media. This finding concurs with the general consensus in literature; i.e., brominated compounds appear more susceptible to photodecomposition than their non-substituted counterparts (Wang et al., 2012; Cruz et al., 2004; Eriksson et al., 2001a). Additionally, Table 1 indicates that, the presence of an aqueous medium does not induces any effect on the geometrical parameters of non-halogenated compounds.

Overall, values in Table 1 clearly establish the anticipated C-Br bond elongation induced by the $S_0 \rightarrow S_1$ transition; i.e., the rate-determining step in the photodecomposition process of

BFRs (Zeng, 2007). The removal of the weakened Br atom (i.e., the atom associated with the highest photoreactivity) upon photodecomposition paves the way for the subsequent hydrogenation (formation of lower brominated congeners) observed experimentally (Fang et al., 2008; Christiansson et al., 2009; Mas et al., 2008). We report that, in all brominated compounds, the degree of elongation for C-Br bond follows the sequence of *ortho* > *meta* > *para* positions. The aromatic compounds that entail a higher degree of bromination experience more C-Br bond elongation in their first excited state for both gaseous and aqueous media. In other words, the lower-brominated congeners demonstrate less C-Br bond stretching in comparison to the higher brominated congeners. Consequently, higher brominated congeners undergo reductive debromination more readily than the lower brominated isomers, in accord with the experimental results of Fang et al (2008).

3.2. Frontier molecular orbitals and the HUMO-LUMO energy gap

The difference in energy ($E^{H\text{-}L}$) between the highest occupied molecular orbital (HOMO) and the lowest unoccupied molecular orbital (LUMO) constitutes an illuminating molecular descriptor of the photoreactivity of molecules (Klán and Wirz, 2009; Zhao and Han, 2009). The $E^{H\text{-}L}$ values dictate the movement of an electron from HOMO to LUMO during the $S_0 \rightarrow S_1$ shift (Fang et al., 2008; Zhao and Han 2009). Fang et al., (2009) established a negative correlation between the energy gap, $E^{H\text{-}L}$, and the photolytic reactivity, log *k*, for PBDE congeners in various media, including gaseous phase and hexane solvent. The decrease of the $E^{H\text{-}L}$ correlates linearly with the increase in the photoreactivity.

Figs. S1 and S2 in the supplementary information depict HOMO and LUMO orbitals for all considered molecules, both in gaseous and aqueous media. Inspection of Fig. S1 reveals molecular fragments involved in the excitation process. The transitions from HOMO to LUMO for all aromatic compounds generally display $\pi \rightarrow \pi^*$ or $\pi \rightarrow \sigma^*$ character. The charge density in the HOMO of the departure state distributes itself over the entire aromatic rings, except for the photoexcitation of brominated congeners of cyclododecane that promotes the *n* electrons. Conversely, the LUMO of the arrival state features either π^* or σ^* character. In the molecules of brominated congeners of biphenyls, diphenylethers, non-brominated biphenyls and diphenyl ether, BMBPE, TBBA, DBBA and bisphenol A, the HOMO and LUMO orbitals are of $\pi \rightarrow \pi^*$ character, with the charge density of the LUMOs spreading itself over the entire aromatic rings.

Fig. S1 portrays the HOMO-LUMO transitions for TriBBA, BTBPE, BDBPE and cyclododecane molecules that display $\pi \rightarrow \sigma^*$ character. For brominated cyclododecane this transition involves promotion of electrons from *n* to σ^* orbitals. The LUMO rests on either the entire molecule (cyclododecane), on one phenyl group (TriBBA, BTBPE and BDBPE), or on a part of molecule (HBCD, TBCD and DBCD). Our calculated HOMO-LUMO orbital transitions for the molecular fragments of DBDE congeners accord with other TDDFT studies (Zhao et al., 2008; Wang et al., 2012; Pan and Bian, 2013).

Fig. 2 presents a linear negative correlation between the number of bromine substituents and $E^{H\text{-}L}$ for the considered BFRs and their non-brominated congeners for both gaseous and aqueous media. Calculated $E^{H\text{-}L}$ values fall in a range of 1.86 – 4.95 eV for gaseous and aqueous configurations, except for those of cyclododecanes that peak around 8.06 eV. The non-aromatic structure of cyclododecane rationalises the noticeable difference in the $E^{H\text{-}L}$

values (Rai et al., 2007; Kornilovich et al., 2003). Bromine substitution in HBCD significantly reduces the $E^{H\text{-}L}$ value to 4.44 eV and 4.49 eV in gaseous and aqueous media, respectively, in reference to the non-brominated cyclododecane, i.e., 8.06 eV (in gaseous phase) and 8.09 eV (in aqueous medium). It follows that, two factors contribute to the high value of $E^{H\text{-}L}$ for cyclododecane: its non-aromatic structure and the absence of bromine substituents.

In the case of PBDEs, the $E^{H\text{-}L}$ amounts to 2.69 eV for diphenylether substituted with 6 bromine atoms increasing to 3.74 eV for DBDE. Additionally, the values of the energy gap for all brominated species fall below those of their non-brominated homologues, in both media. The HBB displays the lowest values of $E^{H\text{-}L}$ of 1.86 eV and 1.48 eV in gaseous and aqueous media, respectively. These values are significantly lower than those for non-halogenated biphenyls, i.e., 3.39 eV (in gaseous phase) and 3.41 eV (in aqueous phase). This finding concurs with the consensus in literature that, the photoreactivity correlates positively with the degree of bromination. Furthermore, the energy gap exhibits a negative linear relationship with the degree of bromination within each group of congeners (Wang et al., 2012; Saeed et al., 2015). Thus, we conclude that, higher brominated congeners demonstrate increased susceptibility towards photodecomposition owing to the lower $E^{H\text{-}L}$ values. Our $E^{H\text{-}L}$ energy analysis coincides with the theoretical predictions of $E^{H\text{-}L}$ for PBDE congeners (Wang et al., 2012; Luo et al., 2015). Overall, the medium (gaseous phase versus water solvent) induces a minor influence on the $E^{H\text{-}L}$ energies, in accord with previous theoretical findings on HBCDs of Zhao et al. (2010) and PBDEs of Wang et al. (2012).

3.3 Charge distribution

We computed the partitioning of electronic density in considered brominated and non-brominated compounds based on the Hirshfeld partitioning formalism (Hirshfeld, 1977; Wiberg and Rablen, 1993). This formalism provides a robust methodology for estimating atomic charges that is insensitive to the deployed basis set, in comparison with the commonly deployed Mulliken population analysis (Guerra et al., 2004; Davidson and Chakravorty, 1992). Table 2 depicts atomic charges on selected positions in all title compounds for the S_0 gaseous state while Fig. S3 draws atomic charge contours for selected molecules. Charges on the bromine atoms (q_{Br}) substituted at different positions in molecule provide a measure of the extent of photoreactivity at *ortho*, *meta* and *para* sites with regard to the C-C/C-O linkages and the OH group. The higher the charge on bromine atom (q_{Br}), the more propensity for the Br atom to depart the molecule via photodecomposition (Fang et al., 2009; Xie et al., 2009; Wang et al., 2012). The most photoreactive bromine atom holds the most positive charge in the gaseous ground state.

The results of charge analysis agree with the data of the earlier theoretical investigations (Eriksson et al., 2004; Wang et al., 2012). The carbon atoms attached to bromine atoms are richer in electrons, therefore, carrying a negative charge. Fig. 3 displays a positive correlation between the atomic charges of Br atom (q_{Br}) in the S_0 state and elongation of C-Br bond lengths in the S_1 state for selected compounds, in both media. We find that, the bromine atom with the highest positive charge in the ground state experiences the maximum elongation in C-Br bond length upon excitation; i.e., for the $S_0 \rightarrow S_1$ transition. For example, in S_0 state of the TBDE and BTBPE molecules, the bromine atom at *ortho* positions (with respect to C-O linkage) endures the highest positive charge of 0.086 *e* and 0.089 *e*, correspondingly (refer to Table 2)

and hence the longest C-Br elongation upon excitation (in the S_1 state). Similarly, in ground state of the TriBBA molecule, bromine atoms substituted at the *ortho*-C(Br) positions (with respect to the hydroxyl group) bear the utmost positive atomic charge of 0.076 *e* (most photoreactive Br atoms) and displays the maximum elongation in C-Br bond of 9.0 % in the first excited state. Overall, the photoreactivity of compounds increases with the degree of bromination, driven by a descending trend in $E^{H\text{-}L}$ energy gap and larger q_{Br} values.

3.4. Optical properties including UV-Vis absorption spectra, excitation energies and oscillation strengths

Molecules absorb the light photons in a discrete bundle of electromagnetic radiation (e.g., as sunlight). The energy of photons corresponding to visible or ultraviolet light is adequate to disrupt or rearrange the covalent bond, accelerate the photochemical process and generate the transient excited states that transform reactants into distinct products (Becker, 1971; Jackson, 1991). Photocatalysts shift the absorption of light from the UV region to the visible-light region, allowing more photons to be absorbed to induce the photochemical reactions. For this reason, in this contribution, we compute the photochemical properties such as excitation energies, oscillation strength and UV-Vis absorption spectra of the selected BFRs and their non-brominated counterparts. To establish an accuracy benchmark of theoretically obtained quantitates, we measure experimentally the UV-Vis spectra of TBBA in hexane and bisphenol A in methanol. This allows us to compare the maximum absorption wavelengths collected in the experiments in the UV-Vis range with those corresponding the highest oscillator strengths, as estimated in the computations.

Tables 3 and 4 present the results of calculated excitation energies (in eV) and oscillator strengths (*f*) for the five lowest excited states of selected brominated and non-brominated molecules in the gaseous and aqueous phase, respectively. Oscillator strength represents the probability of a chemical moiety to absorb or emit electromagnetic radiations to trigger electron transitions between two energy levels. Our computed results illustrate minor differences in excitation energies and oscillator strengths for all brominated and non-brominated congeners, in gaseous and aqueous media. The electron transition probabilities for $S_0 \rightarrow S_3$ energy levels for DBB, HBB, DBDE, HBDE, bisphenol A, TriBBA, BTBPE, TBCD and HBCD appear much higher in comparison to the other energy transitions. Similarly, based on the values of oscillator strength, $S_0 \rightarrow S_2$ represents the most accessible transition in biphenyl, $S_0 \rightarrow S_5$ in TBDE, diphenylether, DBBA, bisphenoxyethane and BMBPE, and $S_0 \rightarrow S_4$ in TBBA and DBCD.

Fig. 4 plots the excitation energy against the $E^{H\text{-}L}$ energy gap. In the case of non-brominated biphenyl, the excitation energy attains a value 4.16 eV (with $E^{H\text{-}L}$ at 3.39 eV). This value surpasses considerably that associated with HBB of 2.35 eV (with $E^{H\text{-}L}$ at 1.86 eV). For HBCD, the required excitation energy amounts to 5.12 eV (with $E^{H\text{-}L}$ at 4.44 eV); i.e., significantly lower in contrast to cyclododecane that necessitates the excitation energy of 8.12 eV (with $E^{H\text{-}L}$ at 8.06 eV). Thus, we conclude that, with the increase in the number of bromine substituents, the excitation energy decreases as function of the $E^{H\text{-}L}$ energy gap. Fig. 5a depicts the negative correlation between the number of bromine atoms and the excitation energy in agreement with the trend portrayed in Fig. 2 (between $E^{H\text{-}L}$ and the number of bromine atoms). In an analogy to this finding, our recent theoretical investigation on bromophenols (Saeed et al., 2015) predicted that, bromophenol congeners with the lowest excitation energy are those with the minimum $E^{H\text{-}L}$ values and the highest number of bromine substituents.

The absorption of electromagnetic waves depends on the oscillator strength (Cantle, 1986), and hence we can compare these two quantities directly. Figs. 6 and 7 show the UV-Vis absorption spectra for all selected brominated and non-brominated compounds in the two media. Our calculated UV-Vis absorption spectrum of DBDE agrees well with the analogous experimental absorption spectrum (Marsh et al., 1999; Fang et al., 2009). Oscillator strength for all brominated and non-brominated molecules falls in a region of UV radiations, i.e., 150 – 530 nm wavelength for both media. The optical spectra exhibit similar shapes in both gaseous and aqueous media for most compounds except for DBB, HBB and DBDE. These compounds display two intensive absorbance bands in aqueous phase, but only one in the gaseous phase. For example, for DBB, we observe one intense peak at a wavelength near 300 nm in the gaseous phase and two peaks in the aqueous phase at wavelengths of 240 nm and 300 nm. Nevertheless, for brominated compounds in the aqueous phase, the band of oscillator strength exhibits a slight blue shift (shifts towards the region of shorter wavelength) in contrast to the gaseous phase. For instance, the strongest band for a gaseous phase HBB occurs at a wavelength of 528 nm, reduced by 25 nm in the aqueous phase. Furthermore, we observe that, brominated compounds demonstrate low excitation energies and intense bands of oscillator strengths at longer wavelengths in contrast to non-brominated molecules.

Fig. 8 compares the experimental measurements of the maximum absorbance of UV-Vis radiation (λ_{max}) with the maximum oscillator strength, as obtained from computations. For a TBBA solution in hexane, the value of theoretically estimated λ_{max} of 293 nm falls close to the experimentally measured value of λ_{max} of 292 nm. Similarly, bisphenol A in methanol exhibits the highest absorption peak at 283 nm in accord with the experimentally-observed estimate of 279 nm. It follows that, the theoretically computed spectrum of oscillator strengths reasonably

match the experimentally measured the absorbance spectrum, especially in terms of the location of the maximum peaks. However, it must be noted that, the calculated wavelength domain is somehow more extended in reference to experimental values. A similar discrepancy between computed and experimental shape of UV-Vis spectra has also been observed by Deblonde et al. (2015) who contrasted experimental and calculated spectra for hexaniobate and hexatantalate ions. The computational cost associated with the size of the investigated BFRs has prevented us from calculating the UV-Vis spectra at higher level of theory. Nonetheless, values computed herein using the DMol^3 package were shown to largely reflect the position of the maximum peaks.

Now, we turn our attention to explain the effect of degree of bromination on the photolytic properties of the studied molecules. Fig. 5 portrays the relationship between the number of bromine atoms and the peak wavelength of the absorption bands. The figure discloses that, as the degree of bromination increases, the highest absorption peaks shift towards the region of longer wavelength for both gaseous and aqueous media, except for DBB. For example, non-brominated biphenyl and HBB display absorption bands at wavelengths of 290 nm and 528 nm, respectively. Likewise, HBCD exhibits an intense absorption peak at a wavelength of 276 nm that shifts towards shorter wavelengths by 42 nm, 56 nm and 130 nm for TBCD, DBCD and cyclododecane molecules, respectively, in the gaseous phase. Accordingly, we conclude that, bromine atoms attached to a molecule play a potent role in altering the photoreactivity of that molecule, by inducing a red shift in the maximum UV absorbance. Analogously, as the number of bromine atoms on the aromatic rings increases, so does the degree of red shift. For instance, six bromine atoms attached to a molecule (HBDE and BTBPE) induce a red shift of 65 nm and 92 nm, respectively, in comparison to two dibrominated molecules (DBDE and BDBPE), as illustrated in Fig. 6. We observe a similar correlation between the red shift in the

absorption peaks and the number of bromine substituents in the aqueous phase. However, the bromination of gaseous molecules induces a more profound red shift. The number of bromine substituents correlates positively with the computed wavelength of maximum absorbance. This observation agrees with the experimental results on the photodecomposition of PBDEs (Eriksson et al., 2004).

A careful examination of the absorption spectra for non-brominated compounds in both gaseous and aqueous media indicates that, in the absence of halogen atom in aromatic compounds, the absorption bands do not exhibit any shift when switching from gaseous to aqueous media. For example; biphenyl molecule unveils three absorption peaks with maximum intensity obtained at 191 nm, 242 nm and 290 nm in both aqueous and gaseous mediums.

4. Conclusion

The results of the present study indicate correlations between geometric and electronic properties that reflect the photoreactive nature of halogenated aromatic molecules. Compounds with the highest degree of bromination entail the lowest values of $E^{H\text{-}L}$ that necessitate the lowest excitation energies for state transitions, exhibiting red shifts for the position of the maximum absorption peaks in the UV-Vis spectra. Our experimentally measured maxima in UV-Vis spectra concur with the location of the theoretically computed wavelengths of the oscillator strengths. Bromine atoms attached to *ortho*-C (with respect to C-C and C-O linkages or the hydroxyl groups) hold the highest positive atomic charges and thus experience the most significant lengthening of the C-Br bonds in their first excited states, in both media, prompting

their preferential debromination. On the other hand, the analogous non-brominated aromatic hydrocarbons possess the highest $E^{H\text{-}L}$ excitation energies and display maximum absorption peaks at shorter wavelengths, indicating their relative stability against photodecomposition. The computed values of $E^{H\text{-}L}$ for selected BFRs and their non-brominated congeners reveal that, the number of bromine substituents and the nature of molecular structure (especially, present of lack of aromaticity) significantly affects the photoreactivity of molecules.

Conflict of interest: The authors declare that they have no conflict of interest.

Acknowledgments

This study has been supported by the Australian Research Council (ARC), and grants of computing time from the National Computational Infrastructure (NCI), Australia as well as the Pawsey Supercomputing Centre in Perth. A.S. and K.S. thank Murdoch University for the postgraduate research scholarships.

References

Alaee, M., Arias, P., Sjödin, A., Bergman, Å., 2003. An overview of commercially used brominated flame retardants, their applications, their use patterns in different countries/regions and possible modes of release. Environ. Int. 29, 683-689.

Ali, N., Harrad, S., Goosey, E., Neels, H., Covaci, A., 2011a. "Novel" brominated flame retardants in Belgian and UK indoor dust: Implications for human exposure. Chemosphere 83, 1360-1365.

Ali, N., Harrad, S., Muenhor, D., Neels, H., Covaci, A., 2011b. Analytical characteristics and determination of major novel brominated flame retardants (NBFRs) in indoor dust. Anal. Bioanal. Chem. 400, 3073-3083.

Altarawneh, M., Dlugogorski, B.Z., 2013. A mechanistic and kinetic study on the formation of PBDD/Fs from PBDEs. Environ. Sci. Technol. 47, 5118-5127.

Altarawneh, M., Dlugogorski, B.Z., 2014a. Thermal decomposition of 1,2-bis(2,4,6-tribromophenoxy)ethane (BTBPE), a novel brominated flame retardant. Environ. Sci. Technol. 48, 14335-14343.

Altarawneh, M., Dlugogorski, B.Z., 2014b. Mechanism of thermal decomposition of tetrabromobisphenol A (TBBA). J. Phys. Chem. A. 118, 9338-9346.

Altarawneh, M., Dlugogorski, B.Z., 2015. Formation of polybrominated dibenzofurans from polybrominated biphenyls. Chemosphere 119, 1048-1053.

Barontini, F., Cozzani, V., Marsanich, K., Raffa, V., Petarca, L., 2004. An experimental investigation of tetrabromobisphenol A decomposition pathways. J. Anal. Appl. Pyrolysis. 72, 41-53.

Barontini, F., Cozzani, V., 2006. Formation of hydrogen bromide and organobrominated compounds in the thermal degradation of electronic boards. J. Anal. Appl. Pyrolysis. 77, 41-55.

Becker, R.S., 1971. Photochemical process. U.S. Pat. 3,567,605.

Buser, H.R., 1986. Polybrominated dibenzofurans and dibenzo-*p*-dioxins: thermal reaction products of polybrominated diphenyl ether flame retardants. Environ. Sci. Technol. 20, 404-408.

Cantle, J. E., 1986. Atomic Absorption Spectyrometry. Elsevier Science, Vol 5.

Chatterjee, D., Dasgupta, S., 2005. Visible light induced photocatalytic degradation of organic pollutants. J. Photochem. Photobiol. C: Photochem. Rev 6, 186-205.

Choi, K.-I., Lee, S.-H., Osako, M., 2009. Leaching of brominated flame retardants from TV housing plastics in the presence of dissolved humic matter. Chemosphere 74, 460-466.

Christiansson, A., Eriksson, J., Teclechiel, D., Bergman, Å., 2009. Identification and quantification of products formed via photolysis of decabromodiphenyl ether. Environ. Sci. Pollut. Res. 16, 312-321.

Covaci, A., Voorspoels, S., de Boer, J., 2003. Determination of brominated flame retardants, with emphasis on polybrominated diphenyl ethers (PBDEs) in environmental and human samples-a review. Environ. Int. 29, 735-756.

Covaci, A., Harrad, S., Abdullah, M. A.E., Ali, N., Law, J. R., Herzke, D., de Wit, C. A., 2011. Novel brominated flame retardants: A review of their analysis, environmental fate and behaviour. Environ. Int. 37, 532-556.

Cruz, J.B., Jafvert, C. T., Hua, I., 2004. Solar photodecomposition of decabromodiphenyl ether: products and quantum yield. Environ. Sci. Technol. 38, 4149-4156.

Darnerud, P.O., 2003. Toxic effects of brominated flame retardants in man and in wildlife. Environ. Int. 29, 841-853.

Davidson, E.R., Chakravorty, S., 1992. A test of the Hirshfeld definition of atomic charges and moments. Anal. Chim. Acta. 83, 319-330.

Deblonde, J.-P.G., Moncomble, A., Cote, G., Bélair, S., Chagnes, A., 2015. Experimental and computational exploration of the UV-visible properties of hexaniobate and hexatantalate ions. RSC Adv., 5, 7619-7627.

de Wit, C.A., 2002. An overview of brominated flame retardants in the environment. Chemosphere 46, 583-624.

Delley, B., 1990. An all-electron numerical method for solving the local density functional for polyatomic molecules. J. Chem. Phys. 92, 508-517.

Delley, B., 2000. From molecules to solids with the $DMol^3$ approach. J. Chem. Phys. 113, 7756-7764.

Delley, B., 2010. Time dependent density functional theory with $DMol^3$. J. Phys.: Condens. Matter. 22, 384208.

Eguchia, A., Isobea, T., Ramua, K., Tuea, N. M., Sudaryantoa, A., Devanathana, G., Vietd, P.H., Tanae, R.S., Takahashia, S., Subramaniana, A., Tanabea, S., 2013. Soil contamination by brominated flame retardants in open waste dumping sites in Asian developing countries. Chemsophere 90, 2365-2371.

Eljarrat, E., de la Cal, A., Raldua, D., Duran, C., Barcelo, D., 2005. Brominated flame retardants in Alburnus from Cinca River Basin (Spain). Environ. Pollut. 133, 501-508.

Eriksson, J., Jakobsson, E., Marsh, G., Bergman, A., 2001a. Photodecomposition of brominated diphenylethers in methanol/water [Abstract]. Presented at the Second International Workshop on Brominated Flame Retardants, 14–16 May,Stockholm, Sweden.

Eriksson, J., Eriksson, L., 2001. 2,2′,6,6′-Tetrachloro-4,4′-propane-2,2-diyldiphenol, 2,2′,6-tribromo-4,4′-propane-2,2-diyldiphenol and 2,2′,6,6′-tetrabromo-4,4′-propane-2,2-diyldiphenol. Acta Crystallogr. C 57, 1308-1312.

Eriksson, J., Green, N., Marsh, G., Bergman, Å., 2004. Photochemical decomposition of 15 polybrominated diphenyl ether congeners in methanol/water. Environ. Sci. Technol. 38, 3119-3125.

Eriksson, P., Jakobsson, E., Fredriksson, A., 2001. Brominated flame retardants: a novel class of developmental neurotoxicants in our environment? Environ Health Perspect. 109, 903-908.

Fang, L., Huang, J., Yu, G., Li, X., 2009. Quantitative structure–property relationship studies for direct photolysis rate constants and quantum yields of polybrominated diphenyl ethers in hexane and methanol. Ecotoxicol. Environ. Saf. 72, 1587-1593.

Fang, L., Huang, J., Yu, G., Wang, L., 2008. Photochemical degradation of six polybrominated diphenyl ether congeners under ultraviolet irradiation in hexane. Chemosphere 71, 258-267.

Fonseca, C. G., Handgraaf, J.W., Baerends, E.J., Bickelhaupt, F.M. 2004. Voronoi deformation density (VDD) charges: Assessment of the Mulliken, Bader, Hirshfeld, Weinhold, and VDD methods for charge analysis. J. Comput. Chem 25, 189-210.

Fromme, H., Hilger, B., Kopp, M., Völkel, W.M., 2014. Polybrominated diphenyl ethers (PBDEs), hexabromocyclododecane (HBCD) and “novel” brominated flame retardants in house dust in Germany. Environ. Int. 64, 61-68.

Guerra, F. C., Handgraaf, J.W., Baerends, E.J., Bickelhaupt, F.M., 2004. Voronoi deformation density (VDD) charges: assessment of the mulliken, bader, hirshfeld, weinhold, and VDD methods for charge analysis. J. Comput. Chem. 25, 189-210.

Gullett, B.K., Linak, W.P., Touati, A., Wasson, S.J., Gatica, S., King. C.J., 2007. Characterization of air emissions and residual ash from open burning of electronic wastes during simulated rudimentary recycling operations. J. Mater. Cycles Waste Manage. 9, 69-79.

Heeb, N.V., Schweizer, W. B., Kohler, M., Gerecke, A.C., 2005. Structure elucidation of hexabromocyclododecanes –a class of compounds with a complex stereochemistry. Chemosphere 61, 65-73.

Hirshfeld, F.L., 1977. Bonded-atom fragments for describing molecular charge densities. Theoretica chimica acta 44, 129-138.

Jackson, D.P., 1991. Dense phase gas photochemical process for substrate treatment. Google Patent.

Jaward, F.M., Farrar, N.J., Harner, T., Sweetman, A.J., Jones, K.C. 2004. Passive air sampling of PCBs, PBDEs, and organochlorine pesticides across Europe. Environ. Sci. Technol. 38, 34−41.

Joschek, H.I., Miller, S.I., 1966. Photocleavage of phenoxyphenols and bromophenols. J. Am. Chem. Soc. 88, 3269-3272.

Klamt, A., 1995. Conductor-like screening model for real solvents: A new approach to the quantitative calculation of solvation phenomena. J. Phys. Chem. 99, 2224-2235.

Klamt, A., Schüürmann, G., 1993. COSMO: a new approach to dielectric screening in solvents with explicit expressions for the screening energy and its gradient. J. Chem. Soc. Perkin. Trans. 2, 799-805.

Kornilovich, P., Bratkovski, A.M., Chang, S.C., Williams, R.S., 2003. Low-forward-voltage molecular rectifier. U.S. Pat. 6670631 B2.

Li, A., Tai, C., Zhao, Z., Wang, Y., Zhang, Q., Jiang, G., Hu, J., 2007. Debromination of decabrominated diphenyl ether by resin-bound iron nanoparticles. Environ. Sci. Technol. 41, 6841-6846.

Luijk, R., Govers, H.A.J., 1992. The formation of polybrominated dibenzo-p-dioxins (PBDDs) and dibenzofurans (PBDFs) during pyrolysis of polymer blends containing brominated flame retardants. Chemosphere 25, 361-374.

Luo, J., Hu, J., Wei, X., Li, L., Huang, X., 2015. Excited states and photodebromination of selected polybrominated diphenyl ethers: computational and quantitative structure –property relationship studies. Int. J. Mol. Sci. 16, 1160.

Luda, M.P., Balabanovich, A.I., Camino, G., 2002. Thermal decomposition of fire retardant brominated epoxy resins. J. Anal. Appl. Pyrolysis. 65, 25-40.

Marsh, G., Hu, J., Jakobsson, E., Rahm, S., Bergman, Å., 1999. Synthesis and characterization of 32 polybrominated diphenyl ethers. Environ. Sci. Technol. 33, 3033-3037.

Mas, S., Juan, A. d., Lacorte, S., Tauler, R., 2008. Photodegradation study of decabromodiphenyl ether by UV spectrophotometry and a hybrid hard- and soft-modelling approach. Anal. Chim. Acta. 618,18-28.

Mimmoa, T., Hannb, S., Jaitzb, L., Cescoa, S., Gessac, C.E., Puschenreiterd, M., 2011. Time and substrate dependent exudation of carboxylates by Lupinus albus L. and Brassica napus L. Plant Physiol. Biochem. 49, 1272−1278.

Möller, A., Xie, Z., Sturm, R., Ebinghaus, R., 2011. Polybrominated diphenyl ethers (PBDEs) and alternative brominated flame retardants in air and seawater of the European Arctic. Environ. Pollut. 159, 1577-1583.

Morris, S., Allchin, C.R., Zegers, B.N., Haftka, J.J.H., Boon, J.P., Belpaire, C., Leonards, P.E.G., van Leeuwen, S.P.J., de Boer, J., 2004. Distribution and fate of HBCD and TBBPA brominated flame retardants in north sea estuaries and aquatic food webs. Environ. Sci. Technol. 38, 5497-5504.

Norris, J.M., Ehrmantraut, J.W., Gibbons, C.L., Kociba, R.J., Schwetz, B.A., Rose, J.Q., Humiston, C.G., Jewett, G.L., Crummett, W.B., Gehring, P.J., Tirsell, J.B., Brosier, J.S., 1973. Toxicological and environmental factors involved in the selection of decabromodiphenyl oxide as a fire retardant chemical. Appl. Polym. Symp. 22, 195-219.

Otha, S., Nishimura, H., Nakao, T., Aozasa, O., Miyata, H., 2001. Characterization of the photolysis of Decabromodiphenyl ether and the levels of PBDEs as its photoproducts in atmospheric air of japan. Organohalogen Compd. 52, 321-324

Ortuño, N., Moltó, J., Conesa, J. A., Font, R., 2014. Formation of brominated pollutants during the pyrolysis and combustion of tetrabromobisphenol A at different temperatures. Environ. Pollut. 191, 31-37.

Pan, L., Bian, W., 2013. Theoretical study on the photodegradation mechanism of nona-BDEs in methanol. ChemPhysChem 14, 1264-1271.

Perdew, J.P., Chevary, J.A., Vosko, S.H., Jackson, K.A., Pederson, M.R., Singh, D.J., Fiolhais, C., 1992. Atoms, molecules, solids, and surfaces: Applications of the generalized gradient approximation for exchange and correlation. Phys. Rev. B. 46, 6671-6687.

Petr. K., Jakob.W., 2009. Photochemistry of Organic Compounds. From Concepts to Practice. John Wiley & Sons.

Rai, D., Joshi, H., Kulkarni, A.D., Gejji, S.P., Pathak, R.K., 2007. Electric field effects on aromatic and aliphatic hydrocarbons: a density-functional study. J. Phys. Chem. A. 111, 9111-9121.

Saeed, A, Dlugogorski, B.Z., Altarawneh M., 2015. Formation of brominated and non-brominated species from gas-phase thermal decomposition of pure TBBA. 14th International Congress on Combustion By-Products and Their Health Effects, Umeå, Sweden.

Saeed A., Altarawneh, M., Dlugogorski BZ., 2016a. Formation of PBDD/F precursors in gas-phase decomposition of tetrabromobisphenol A (TBBA). Organohalogen Compd. 78, 672-674.

Saeed, A., Altarawneh, M., Dlugogorski, B.Z., 2016b. Photodecomposition of bromophenols. Chemosphere 150, 749-758.

Sakai, S.-i., Watanabe, J., Honda, Y., Takatsuki, H., Aoki, I., Futamatsu, M., Shiozaki, K., 2001. Combustion of brominated flame retardants and behavior of its byproducts. Chemosphere 42, 519-531.

Sellström, U., Kierkegaard, A., Alsberg, T., Jonsson, P., Wahlberg, C., De Wit, C., 1999. Brominated flame retardants in sediments from europena estuaries, the Baltic Sea and in sewage sludge. Organohalogen Compd. 40, 383-386.

Söderström, G., Sellström, U., de Wit, C.A., Tysklind, M., 2004. Photolytic debromination of decabromodiphenyl ether (BDE 209). Environ. Sci. Technol. 38, 127-132.

Stapleton, H.M., Klosterhaus, S., Keller, A., Ferguson, P.L., Bergen, S.V., Coopert, E., Webster, T.F., Blum, A., 2011. Identification of flame retardants in polyurethane foam collected from baby products. Environ. Sci. Technol. 45, 5323-5331.

Suh, Y.W., Buettner, G.R., Venkataraman, S., Treimer, S.E., Robertson, L.W., Ludewig, G., 2009. UVA/B-induced formation of free radicals from decabromodiphenyl ether. Environ. Sci. Technol. 43, 2581–2588.

Sun, C., Chang, W., Ma, W., Chen, C., Zhao, J., 2013. Photoreductive debromination of decabromodiphenyl ethers in the presence of carboxylates under visible light irradiation. Environ. Sci. Technol. 47, 2370−2377.

Tian, M., Chen, S.J., Wang, J., Zheng, X.B., Luo, X.J., Mai, B,X., 2011. Brominated flame retardants in the atmosphere of e-waste and rural sites in southern china: seasonal variation, temperature dependence, and gas-particle partitioning. Environ. Sci. Technol. 45, 8819-8825.

Wang, S., Hao, C., Gao, Z., Chen, J., Qiu, J., 2012. Effects of excited-state structures and properties on photochemical degradation of polybrominated diphenyl ethers: A TDDFT study. Chemosphere 88, 33-38.

Wang, H., Zhu, C., Yu, J.G., Lin, S. H. 2009. Anharmonic Franck−Condon simulation of the absorption and fluorescence spectra for the low-lying S_1 and S_2 excited states of pyridine. J. Phys. Chem. A. 113, 14407-14414.

Watanabe, I., Sakai, S.I., 2003. Environmental release and behavior of brominated flame retardants. Environ. Int. 29, 665-682.

Watanabe, I., Tatsukawa, R., 2008. Formation of brominated dibenzofurans from the photolysis of flame retardant decabromobiphenyl ether in hexane solution by UV and sun light. Bull. Environ. Contam. and Toxicol. 39, 953-959.

Weber, R., Kuch, B., 2003. Relevance of BFRs and thermal conditions on the formation pathways of brominated and brominated–chlorinated dibenzodioxins and dibenzofurans. Environ. Int. 29, 699-710.

Wiberg, K.B., Rablen, P.R., 1993. Comparison of atomic charges derived via different procedures. J. Comput. Chem. 14, 1504-1518.

Xie, Q., Chen, J., Shao, J., Chen, C.e., Zhao, H., Hao, C., 2009. Important role of reaction field in photodegradation of deca-bromodiphenyl ether: Theoretical and experimental investigations of solvent effects. Chemosphere 76, 1486-1490.

Yao, L., Lin, S.H. 2008. The anharmonic effect study of coupled morse oscillators for the unimolecular reaction. Sci. China, Ser. B, Chem. 51, 1146-1152.

Zangwill, A., Soven, P., 1980. Density-functional approach to local-field effects in finite systems: Photoabsorption in the rare gases. Phys. Rev. A 21, 1561-1572.

Zeng, X., 2007. Development, Validation and the Application of a Congener Specific Photodegradation Model for PBDEs. Oregon State University

Zhao, G.-J., Han, K.L., 2009. Excited state electronic structures and photochemistry of heterocyclic annulated perylene (HAP) materials tuned by heteroatoms: S, Se, N, O, C, Si, and B. J. Phys. Chem. A, 113, 4788-4794.

Zhao, Y.Y., Tao, F.M., Zeng, E.Y., 2008. Theoretical study on the chemical properties of polybrominated diphenyl ethers. Chemosphere 70, 901-907.

Zhao, Y.Y., Zhang, X.H., Sojinu, O.S.S., 2010. Thermodynamics and photochemical properties of a, b, and c-hexabromocyclododecanes: A theoretical study. Chemosphere 80, 150-156.

Zhu, C., Liang, K.K., Hayashi, M., Lin, S.H. 2009. Theoretical treatment of anharmonic effect on molecular absorption, fluorescence spectra, and electron transfer. J. Chem. Phys. 358, 137-146.

Table 1

Comparison of bond lengths (C-Br) for the title BFRs and their non-brominated congeners in the ground (S_o) and excited (S_1) states in both gaseous and aqueous media. Bond lengths are in Å. Atomic positions are shown in Fig. 1.

	Gaseous phase		
Compounds	**Position of C-Br bonds**	**C-Br bond lengths in S_o state**	**C-Br bond lengths in S_1 state**
DBB (4,4′-dibromobiphenyl)	5-4; 5′-4′	1.939; 1.939	2.009; 2.009
TBB (2,2′,4,4′-tetrabromobiphenyl)	3-2; 5-4; 3′-2′; 5′-4′	1.939; 1.939; 1.939; 1.939	1.963; 1.962; 1.963; 1.962
HBB (2,2′,4,4′,6,6′-hexabromobiphenyl)	3-2; 5-4; 7-6; 3′-2′; 5′-4′; 7′-6′	1.955; 1.929; 1.954; 1.955; 1.929; 1954	2.040; 1.985; 2.040; 2.040; 1.985; 2.040
DBDE (4,4′-dibromodiphenylether)	5-4; 5′-4′	1.941; 1.942	2.012; 2.012
TBDE (2,2′,4,4′-tetrabromodiphenylether)	3-2; 5-4; 3′-2′; 5′-4′	1.936; 1.938; 1.934; 1.939	2.038; 2.017; 2.029; 2.011
HBDE (2,2′,4,4′,6,6′-hexabromodiphenylether)	3-2; 5-4; 7-6; 3′-2′; 5′-4′; 7′-6′	1.933; 1.936; 1.927; 1.934; 1.935; 1.928	2.051; 2.023; 2.035; 2.045; 2.022; 2.031
DBBA (2,2′-dibromobisphenol A)	3-2; 3′-2 ′	1.956; 1.954	2.042; 2.050
TriBBA (2,2′,6-tribromobisphenol A)	3-2; 3′-2′; 5′-6′	1.955; 1.934; 1.954	2.132; 2.073; 2.033
TBBA (2,2′,6,6′-tetrabromobisphenol A)	3-2; 5-6; 3′-2′; 5′-6′	1.954; 1.933; 1.953; 1.934	2.010; 2.006; 2.125; 2.061
BMBPE (1,2-bis(4-bromophenoxy)ethane)	5-4; 5′-4′	1.943; 1.943	1.978; 1.978
BDBPE (1,2-bis(2,4-dibromophenoxy)ethane)	3-2; 5-4; 3′-2′; 5′-4′	1.933; 1.940; 1.936; 1.940	2.020; 2.018; 2.008; 2.004
BTBPE (1,2-bis(2,4,6-tribromophenoxy)ethane)	3-2; 5-4; 7-6; 3′-2′; 5′-4′; 7′-6′	1.941; 1.937; 1.930; 1.944; 1.938; 1.913	2.046; 2.032; 2.039; 2.057; 2.026; 2.048
DBCD (1,2-dibromocyclododecane)	3-1; 4-2	2.028; 2.044	2.326; 2.105
TBCD (1,2,5,6-tetrabromocyclododecane)	5-1; 6-2; 7-3; 8-4	2.031; 2.040; 2.042; 2.031	2.215; 2.220; 2.126; 2.107
HBCD (1,2,5,6,9,10-hexabromocyclododecane)	7-1; 8-2; 9-3; 10-4; 11-5; 12-6	2.03; 2.08; 2.028; 2.038; 2.043; 2.028	2.197; 2.104; 2.104; 2.098; 2.118; 2.208
	Position of C-H atoms	**C-H bond lengths in S_o state**	**C-H bond lengths in S_1 state**
Biphenyl	5-4; 5′-4′	1.097; 1.097	1.097; 1.097
Diphenylether	5-4; 5′-4′	1.098; 1.097	1.098; 1.097
Bisphenol A	4-2; 5-6; 4′-2′; 5′-6′	1.10; 1.097; 1.096; 1.10	1.10; 1.097; 1.10; 1.096
Bisphenoxyethane	3-2; 5-4; 7-6; 2′-3′; 5′-4′; 7′-6′	1.096; 1.098; 1.098; 1.098; 1.097; 1.098	1.097; 1.097; 1.095; 1.097; 1.095; 1.094

Cyclododecane	7-1; 8-2; 9-3; 10-4; 11-5; 12-6	1.114; 1.115; 1.114; 1.115; 1.114; 1.115	1.117; 1.115; 1.114; 1.115; 1.114; 1.115
	Solvent phase (aqueous)		
	Position of C-Br atoms	**C-Br bond lengths in S_o state**	**C-Br bond lengths in S_1 state**
DBB	5-4; 5′-4′	1.948; 1.948	2.007; 2.007
TBB	3-2; 5-4; 3′-2′; 5′-4′	1.939; 1.936; 1.939; 1.936	1.945; 1.944; 1.945;1.944
HBB	3-2; 5-4; 7-6; 3′-2′; 5′-4′; 7′-6′	1.941; 1.937; 1.939; 1.940; 1.936; 1.39	2.050; 2.028; 2.050; 2.050; 2.028; 2.050
DBDE	5-4; 5′-4′	1.949; 1.950	2.011; 2.010
TBDE	3-2; 5-4; 3′-2′; 5′-4′	1.939; 1.944; 1.937; 1.944	2.041; 2.020; 2.031; 2.015
HBDE	3-2; 5-4; 7-6; 3′-2′; 5′-4′; 7′-6′	1.935; 1.931; 1.939; 1.935; 1.931; 1.938	2.050; 2.022; 2.038; 2.050; 2.022; 2.038
DBBA	3-2; 3′-2 ′	1.955; 1.955	2.042; 2.050
TriBBA	3-2; 3′-2′; 5′-6′	1.951; 1.943; 1.954	2.131; 2.100; 2.035
TBBA	3-2; 5-6; 3′-2′; 5′-6′	1.950; 1.942; 1.951; 1.942	2.010; 2.006; 2.104; 2.057
BMBPE	5-4; 5′-4′	1.952; 1.952	1.978; 1.978
BDBPE	3-2; 5-4; 3′-2′; 5′-4′	1.940; 1.946; 1.940; 1.947	2.020; 2.018; 2.008; 2.004
BTBPE	3-2; 5-4; 7-6; 3′-2′; 5′-4′; 7′-6′	1.936; 1.939; 1.939; 1.939; 1.939; 1.936	2.020; 2.005; 2.013; 2.042; 2.033; 2.047
DBCD	3-1; 4-2	2.045; 2.064	2.334; 2.125
TBCD	5-1; 6-2; 7-3; 8-4	2.044; 2.056; 2.058; 2.047	2.324; 2.340; 2.234; 2.207
HBCD	7-1; 8-2; 9-3; 10-4; 11-5; 12-6	2.028; 2.031; 2.028; 2.043; 2.038; 2.028	2.196; 2.100; 2.104; 2.009; 2.119; 2.207
	Position of C-H atoms	**C-H bond lengths in S_o state**	**C-H bond lengths in S_1 state**
Biphenyl	5-4; 5′-4′	1.097; 1.097	1.097; 1.097
Diphenylether	5-4; 5′-4′	1.098; 1.097	1.098; 1.097
Phenol	6-2; 7-3; 8-4; 9-5	1.10; 1.098; 1.098; 1.098	1.10; 1.098; 1.098; 1.099
Bisphenol A	4-2; 5-6; 4′-2′; 5′-6′	1.10; 1.097; 1.096; 1.10	1.10; 1.098; 1.097; 1.10
Bisphenoxyethane	3-2; 5-4; 7-6; 2′-3′; 5′-4′; 7′-6′	1.096; 1.098; 1.098; 1.098; 1.097; 1.098	1.099; 1.098; 1.101; 1.100; 1.098; 1.098
Cyclododecane	7-1; 8-2; 9-3; 10-4; 11-5; 12-6	1.114; 1.115; 1.114; 1.115; 1.114; 1.115	1.114; 1.115; 1.114; 1.115; 1.114; 1.115

Table 2

Atomic charges on the selected BFRs**.** The parameter *n* represents the position of oxygen (O), bromine (Br) and carbon (C) atoms with the value of net atomic charge present in the ground state (S_0) in the gaseous phase. Atomic positions are depicted in Fig. 1.

Compounds	***n***	**Atomic charges (S_0)**
DBB	Br(4); Br(4′); C(5); C(5′)	0.0725; 0.0725; -0.0293; -0.0294
TBB	Br(2); Br(2′); Br(4); Br(4′); C(3); C(3′); C(5); C(5′)	0.0802; 0.0802; 0.0721; 0.0721; -0.0323; -0.0322; -0.0295; -0.0295
HBB	Br(2); Br(2′); Br(4); Br(4′); Br(6); Br(6′); C(3); C(3′); C(5); C(5′); C(7); C(7′)	0.0814; 0.0814; 0.0795; 0.0795; 0.0795; 0.0795; -0.0370; -0.0370; -0.0325; -0.0325; -0.0370; -0.0370
DBDE	O(1); Br(4); Br(4′); C(5); C(5′)	-0.1001; 0.0677; 0.0677; -0.0324; -0.0324
TBDE	Br(2); Br(2′); Br(4); Br(4′); C(3); C(3′); C(5); C(5′)	0.0857; 0.0846; 0.0709; 0.0708; -0.0458; -0.0457; -0.0321; -0.0320
HBDE	Br(2); Br(2′); Br(4); Br(4′); Br(6); Br(6′); C(3); C(3′); C(5); C(5′); C(7); C(7′)	0.0845; 0.0843; 0.0731; 0.0733; 0.0799; 0.0799; -0.0466; -0.0467; -0.0326; -0.0325; -0.0446; -0.0445
DBBA	O(1); O(1′); Br(2); Br(2′); C(3); C(3′);	-0.1478; -0.1475; 0.0576; 0.0531; -0.0498; -0.0513;
TriBBA	O(1); O(1′); Br(2); Br(2′); C(3); C(3′); Br(6′); C(5)	-0.1471; -0.1525; 0.0757; 0.0591; -0.0434; -0.0494; 0.0537; -0.0434
TBBA	O(1); O(1′); Br(2); Br(2′); C(3); C(3′); Br(6); Br(6′); C(5); C(5′)	-0.1520; -0.1521; 0.0598; 0.0550; -0.0503; -0.0521; 0.0733; 0.0733; -0.0447; -0.0433
BMBPE	O(1); O(1′); Br(4); Br(4′); C(5); C(5′)	-0.0738; -0.0738; 0.060; 0.060; -0.0348; -0.0348
BDBPE	O(1); O(1′); Br(2); Br(2′); C(3); C(3′); Br(4); Br(4′); C(5); C(5′)	-0.0927; -0.0910; 0.0853; 0.0683; -0.0428; -0.0434; 0.0644; 0.0649; -0.0332; -0.0330
BTBPE	O(1); O(1′); Br(2); Br(2′); C(3); C(3′); Br(4); Br(4′); C(5); C(5′); Br(6); Br(6′); C(7); C(7′)	-0.0990; -0.0935; 0.0668; 0.0719; -0.0433; -0.0442; 0.0663; 0.0675; -0.0334; -0.0348; 0.0881; 0.0888; -0.0435; -0.0404
DBCD	Br(1); Br(2); C(3); C(4)	0.0241; 0.0077; -0.0303; -0.0309
TBCD	Br(1); Br(2); Br(3); Br(4); C(5); C(6); C(7); C(8)	0.0334; 0.0294; 0.0228; 0.0200; -0.0298; -0.0290; -0.0319;-0.0346
HBCD	Br(1); Br(2); Br(3); Br(4); Br(5); Br(6); C(7); C(8); C(9); C(10); C(11); C(12)	0.0366; 0.0250; 0.0416; 0.0276; 0.0298; 0.0372; -0.0271; -0.0282; -0.0280; -0.0343; -0.0289; -0.0312

Table 3

Calculated excitation energies of molecules as photon absorption energy *E* (in eV) and the oscillator strength (*f*) of the five lowest excited states of selected BFRs and their non-brominated congeners in the gaseous phase.

	***E* (in eV)**	***f***	***E* (in eV)**	***f***	***E* (in eV)**	***f***
	biphenyl		**DBB**		**TBB**	
S1	4.16	0.000000	3.17	0.000000	4.12	0.000000
S2	4.27	0.528043	3.79	0.000000	4.18	0.000000
S3	4.44	0.005237	4.13	0.738376	4.26	0.000000
S4	4.82	0.000001	4.13	0.000000	4.35	0.000000
S5	5.09	0.045887	4.25	0.000000	4.40	0.000000
	HBB		**Diphenylether**		**DBDE**	
S1	1.67	0.000000	4.04	0.000000	3.81	0.000000
S2	2.24	0.000000	4.12	0.000000	3.91	0.000000
S3	2.35	0.212599	4.35	0.000000	4.12	0.011069
S4	2.43	0.000000	4.41	0.000000	4.14	0.000000
S5	2.49	0.021078	4.43	0.010764	4.20	0.001869
	TBDE		**HBDE**		**Bisphenol A**	
S1	3.86	0.000000	3.56	0.000000	4.13	0.026168
S2	3.96	0.000000	3.70	0.000000	4.22	0.000329
S3	4.04	0.000000	3.71	0.022974	4.52	0.049700
S4	4.07	0.000000	3.81	0.000272	4.58	0.001626
S5	4.12	0.025349	3.85	0.0000000	4.74	0.010612
	DBBA		**TriBBA**		**TBBA**	
S1	3.93	0.000000	3.83	0.000000	3.72	0.000000
S2	4.02	0.000000	3.95	0.000000	3.75	0.000000
S3	4.07	0.000000	3.95	0.006451	3.79	0.000000
S4	4.18	0.000000	4.01	0.000000	3.84	0.005748
S5	4.23	0.017844	4.04	0.000000	3.86	0.002312
	bisphenoxyethane		**BMBPE**		**BDBPE**	

S1	4.36	0.001883	3.96	0.000000	4.14	0.000000
S2	4.51	0.003150	3.96	0.000000	4.17	0.000000
S3	4.55	0.003084	4.17	0.000000	4.25	0.000000
S4	4.83	0.005917	4.18	0.000000	4.30	0.000000
S5	4.85	0.013199	4.18	0.000315	4.36	0.000000
	TBTBPE		**cyclododecane**		**DBCD**	
S1	3.80	0.000000	8.12	0.023689	5.29	0.000000
S2	3.89	0.000000	8.15	0.000128	5.36	0.000000
S3	3.90	0.000713	8.34	0.003114	5.48	0.000000
S4	3.98	0.000447	8.37	0.000475	5.50	0.003934
S5	3.98	0.000000	8.40	0.009544	5.52	0.000000
	TBCD		**HBCD**			
S1	4.94	0.000000	4.93	0.000000		
S2	5.11	0.000000	5.13	0.000000		
S3	5.13	0.000932	5.13	0.000847		
S4	5.18	0.000000	5.18	0.000000		
S5	5.21	0.000000	5.20	0.000000		

Table 4

Calculated excitation energies of molecules as photon absorption energy *E* (in eV) and the oscillator strength (*f*) of the five lowest excited states of selected BFRs and their non-brominated congeners in the aqueous phase.

	***E* (in eV)**	***f***	***E* (in eV)**	***f***	***E* (in eV)**	***f***
	biphenyl		**DBB**		**TBB**	
S1	4.17	0.000000	4.13	0.756427	4.09	0.000000
S2	4.28	0.527685	4.14	0.000000	4.19	0.000000
S3	4.45	0.005736	4.56	0.000051	4.25	0.000000
S4	4.83	0.000001	4.68	0.000004	4.36	0.000000
S5	5.10	0.041462	4.80	0.000010	4.40	0.000000
	HBB		**diphenylether**		**DBDE**	
S1	1.17	0.000000	4.08	0.000000	4.16	0.009224
S2	1.50	0.000000	4.14	0.000000	4.41	0.001709
S3	1.69	0.008854	4.36	0.000000	4.49	0.254724
S4	1.86	0.000000	4.45	0.000000	4.65	0.001598
S5	1.89	0.000000	4.45	0.011504	4.71	0.000346
	TBDE		**HBDE**		**Bisphenol A**	
S1	3.88	0.000000	3.57	0.000000	4.14	0.025994
S2	3.98	0.000000	3.72	0.024709	4.23	0.000373
S3	4.05	0.000000	3.72	0.000000	4.53	0.051397
S4	4.09	0.000000	3.84	0.000241	4.60	0.001396
S5	4.15	0.024313	3.86	0.000000	4.75	0.010763
	DBBA		**TriBBA**		**TBBA**	
S1	3.95	0.000000	3.83	0.000000	3.82	0.000000
S2	4.00	0.000000	3.93	0.005356	3.84	0.000000
S3	4.05	0.000000	3.94	0.000000	3.96	0.009846
S4	4.20	0.000000	3.97	0.000000	3.96	0.000543
S5	4.24	0.015757	4.05	0.000000	3.97	0.000000
	Bisphenoxyethane		**BMBPE**		**BDBPE**	

S1	4.37	0.001973	3.97	0.000000	3.94	0.000000
S2	4.52	0.003131	3.97	0.000000	3.94	0.000000
S3	4.56	0.003101	4.18	0.000000	4.04	0.000000
S4	4.84	0.005482	4.19	0.000230	4.05	0.000000
S5	4.86	0.014184	4.19	0.000000	4.11	0.000001
	BTBPE		**cyclododecane**		**DBCD**	
S1	3.84	0.000000	8.14	0.023283	5.28	0.000000
S2	3.86	0.000000	8.17	0.000113	5.36	0.000000
S3	3.94	0.003183	8.35	0.003426	5.49	0.004894
S4	4.00	0.000524	8.38	0.000767	5.49	0.000000
S5	4.03	0.000000	8.42	0.009694	5.50	0.000000
	TBCD		**HBCD**			
S1	4.89	0.000000	4.88	0.000000		
S2	5.06	0.000000	5.05	0.000000		
S3	5.11	0.001324	5.09	0.001339		
S4	5.17	0.000000	5.14	0.000000		
S5	5.18	0.000000	5.16	0.000000		

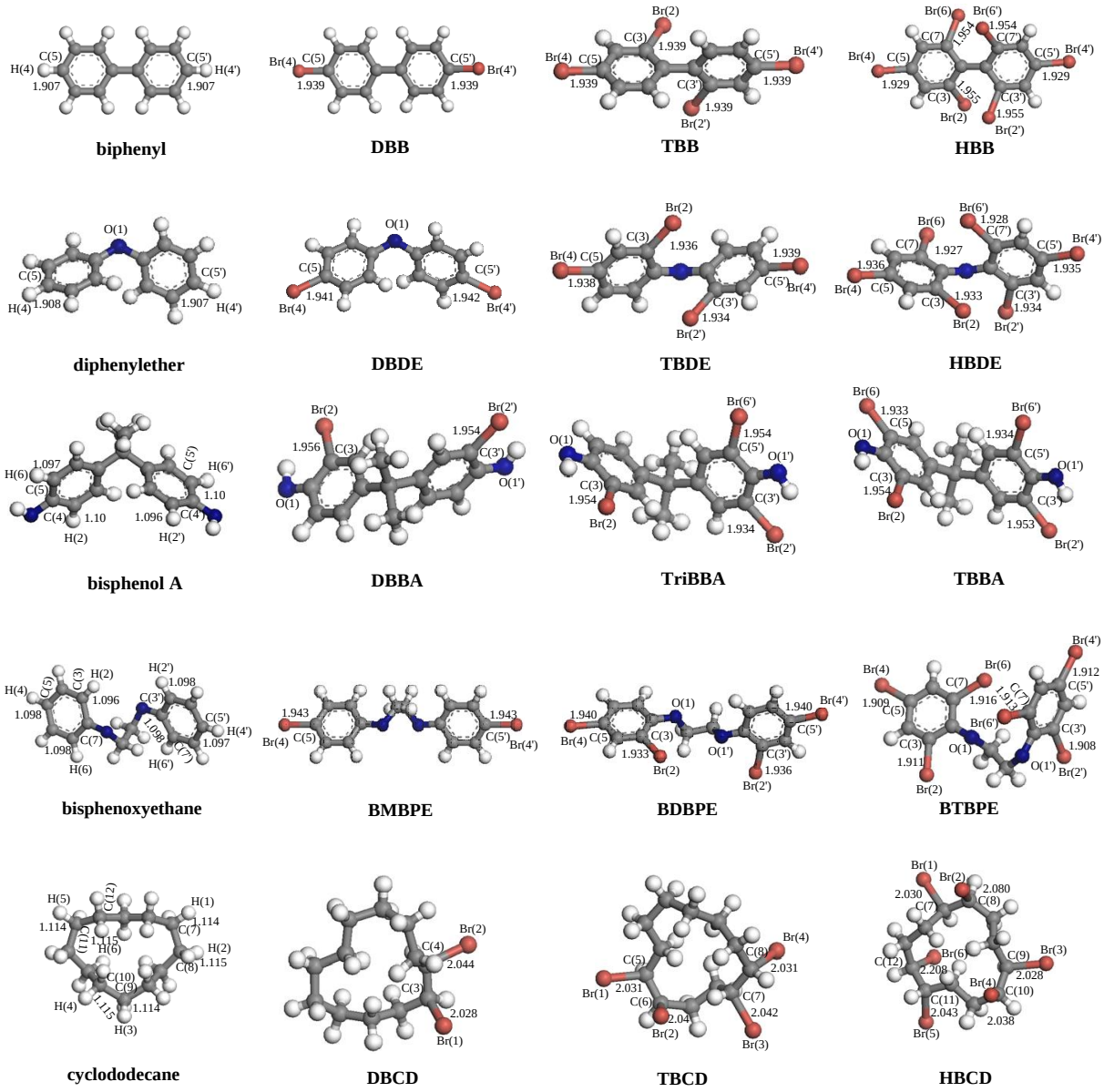

Fig. 1. Optimised geometries of selected BFRs and their non-brominated congeners with C-Br bond distance (in Å) corresponding to the gaseous S_0 state. Bromine and oxygen atoms are denoted by red and blue spheres, respectively.

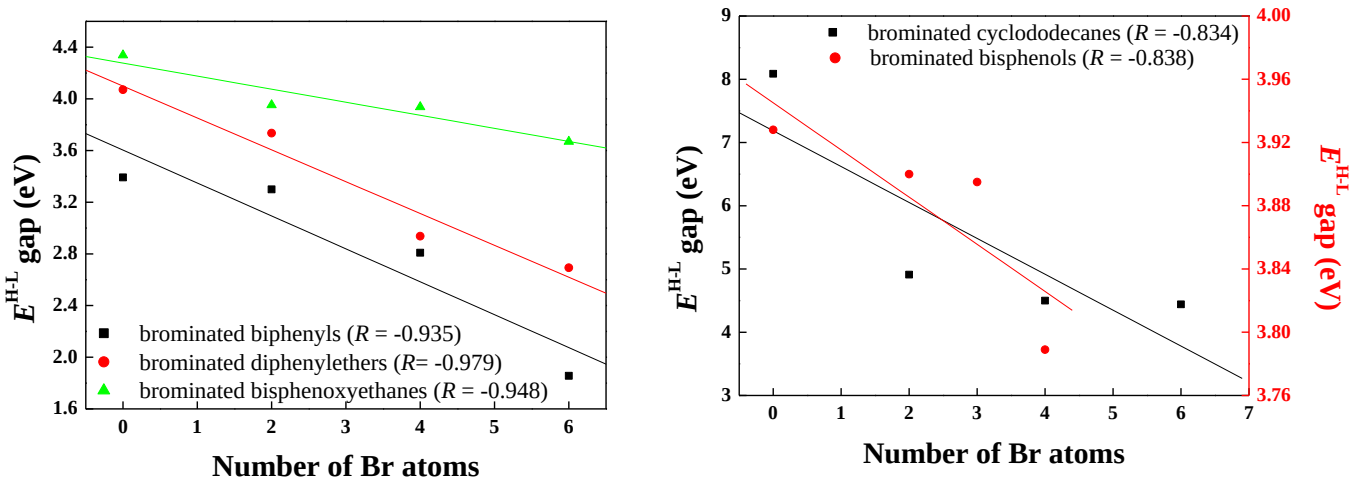

(a)

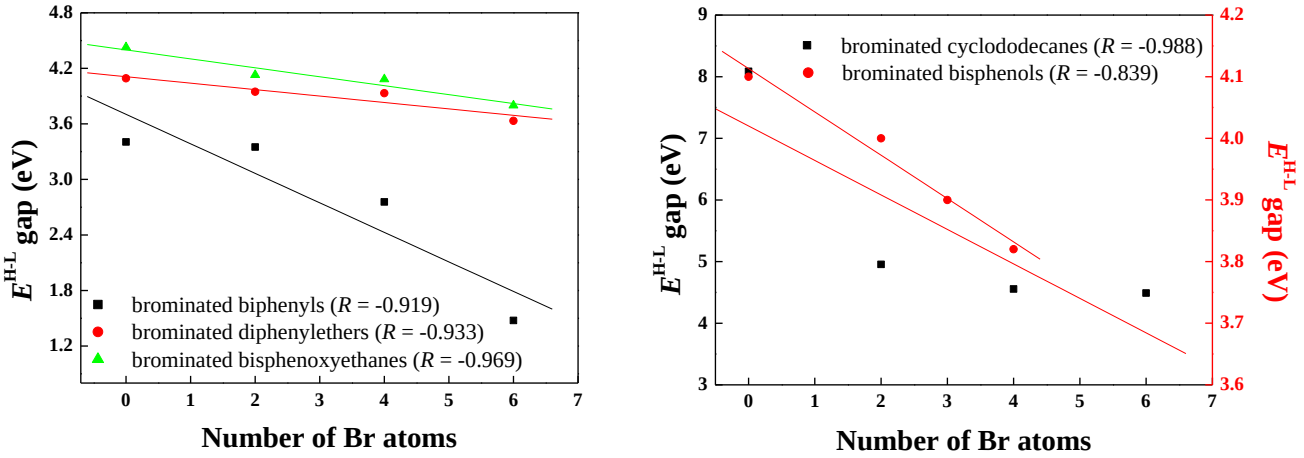

(b)

Fig. 2. Correlation between the number of Br atoms and calculated energy gap $E^{H\text{-}L}$ (in eV) between the frontier molecular orbitals for (a) gaseous and (b) aqueous phases. The value of *R* depicts the degree of linearity of a trend line.

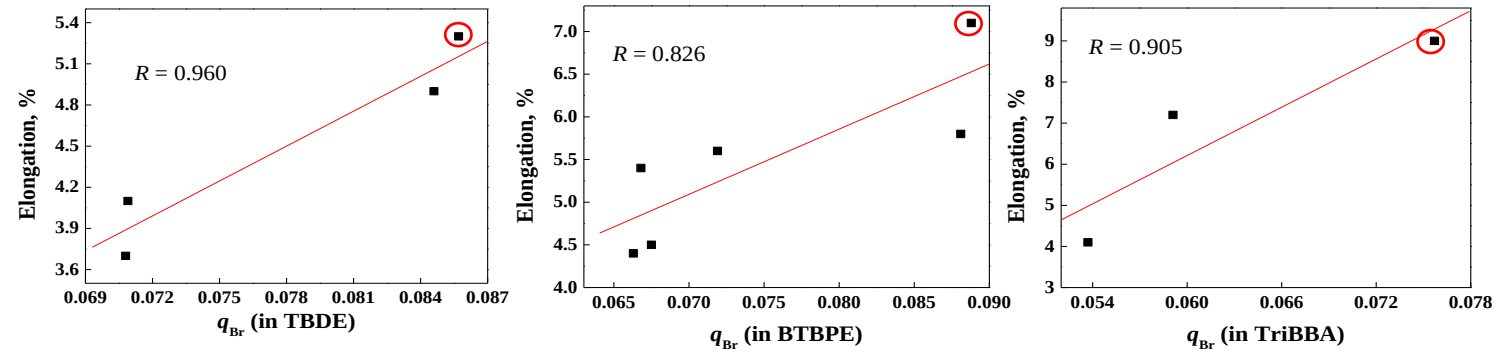

(a)

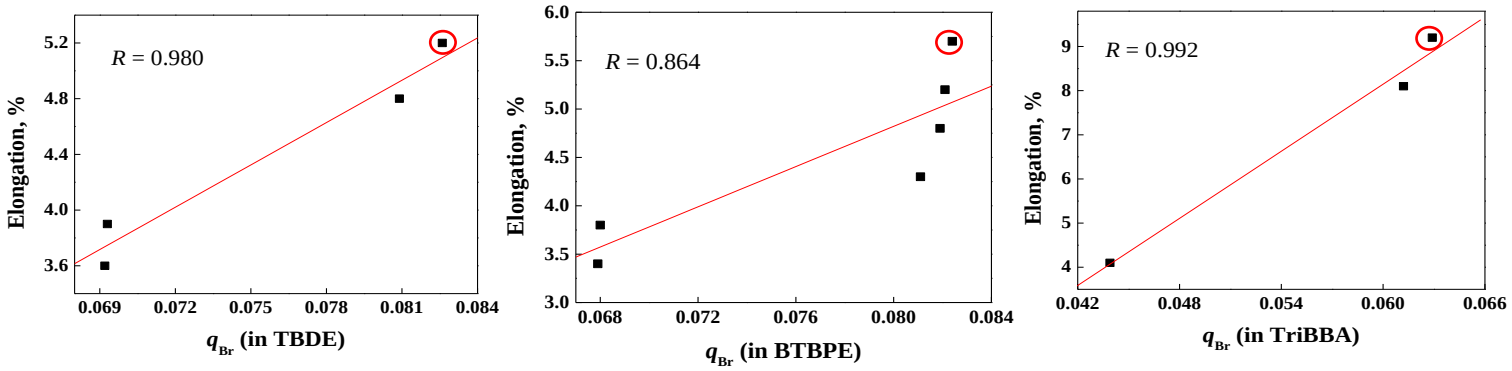

(b)

Fig. 3. Correlations between the calculated atomic charge on bromine (q_{Br}) in the S_0 state and the percentage of elongation in C-Br bond upon the $S_0 \rightarrow S_1$ transition for selected congeners of BFRs in gaseous (a) and aqueous (b) phases. The bromine atom attached at an *ortho* position with regard to the C-O linkage (in TBDE and BTBPE) and hydroxyl group (in TBBA) entails the highest positive charge (encircled in red). The value of *R* depicts the degree of linearity of a trend line.

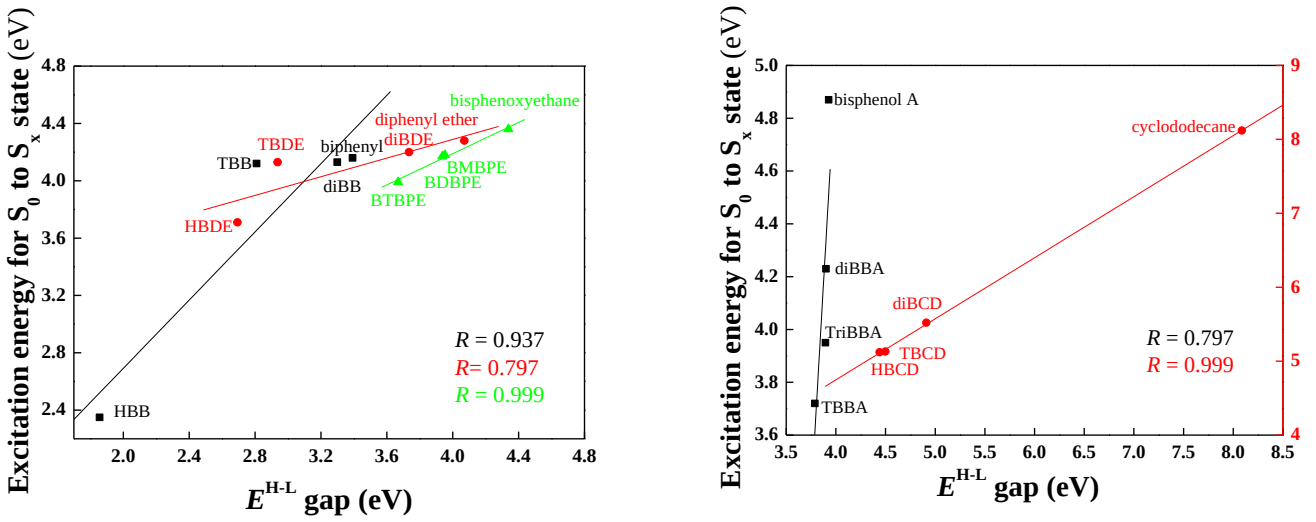

(a)

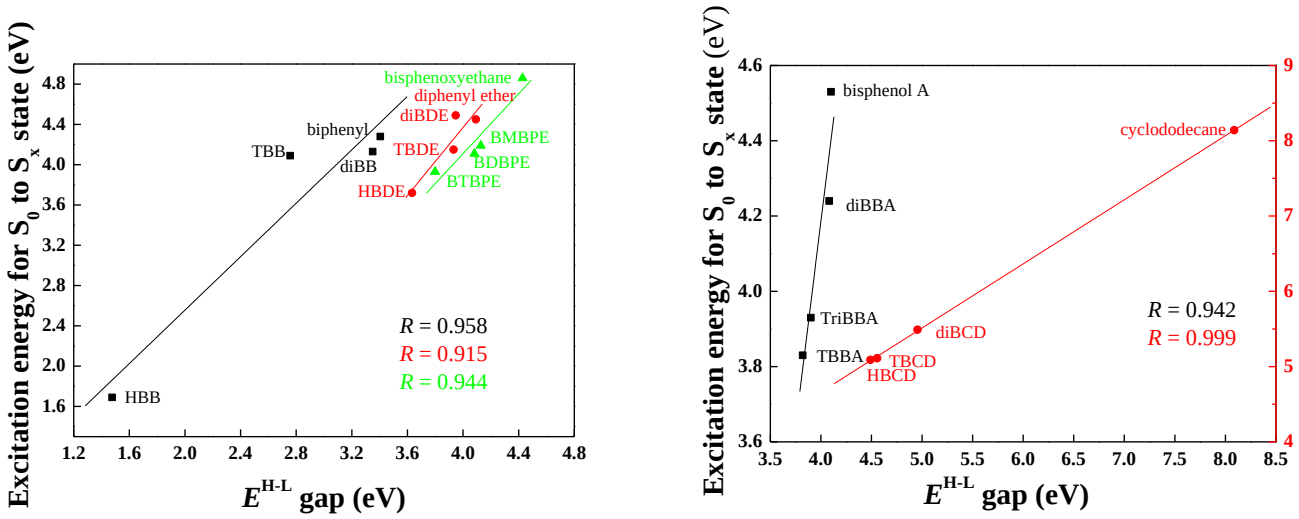

(b)

Fig. 4. Correlation between the $E^{H\text{-}L}$ (in eV) and the excitation energy (in eV) for the $S_0 \rightarrow S_x$ transition for brominated and non-brominated compounds in (a) gaseous and (b) aqueous phases. S_x represents the most accessible excited state. The value of *R* depicts the degree of linearity of a trend line.

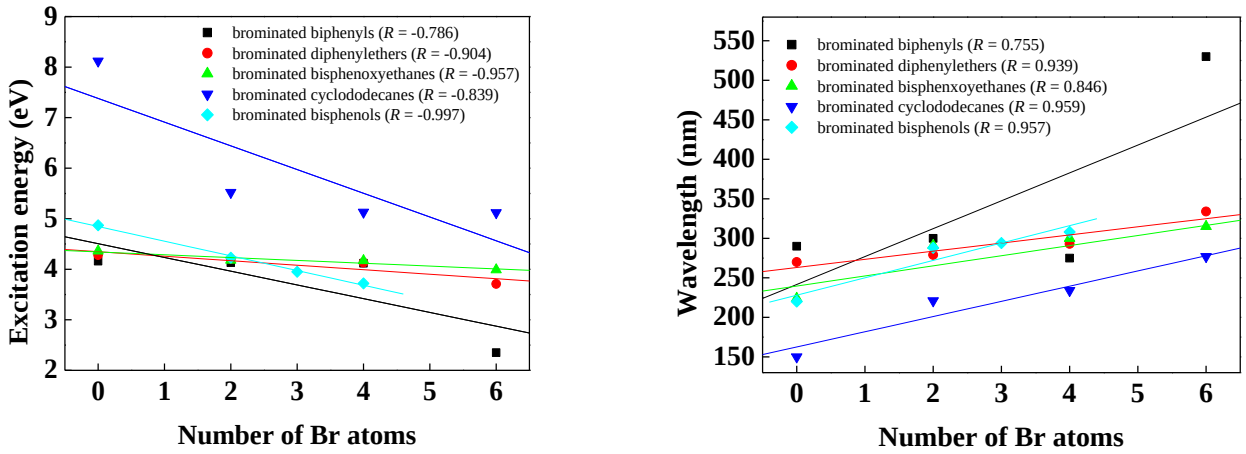

(a)

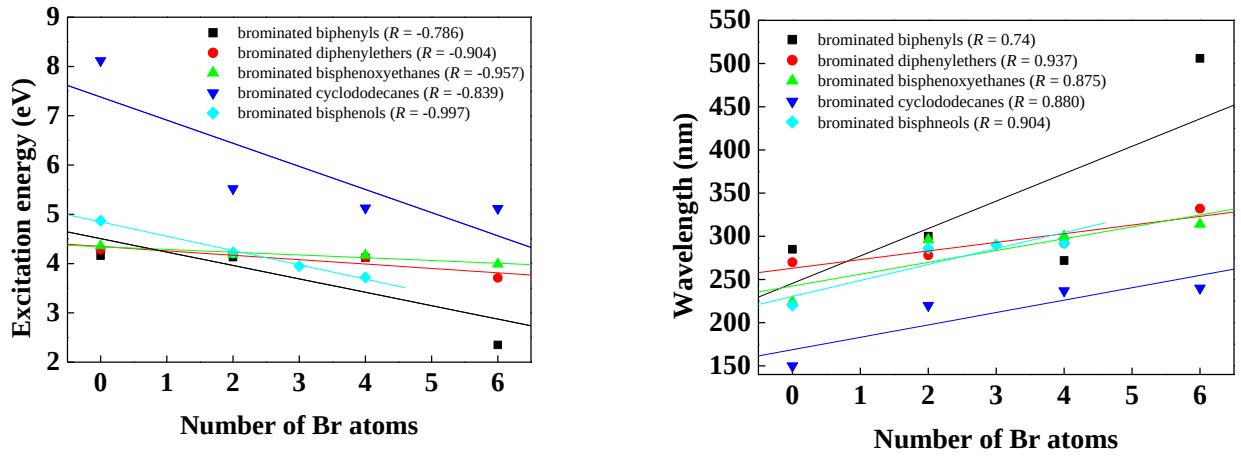

(b)

Fig. 5. Correlation between the calculated lowest excitation energy values (eV) and the number of bromine atoms, as well as between the calculated wavelength (nm) at the maximum absorption and the number of bromine atoms in (a) gaseous and (b) aqueous phases. The value of *R* depicts the degree of linearity of a trend line.

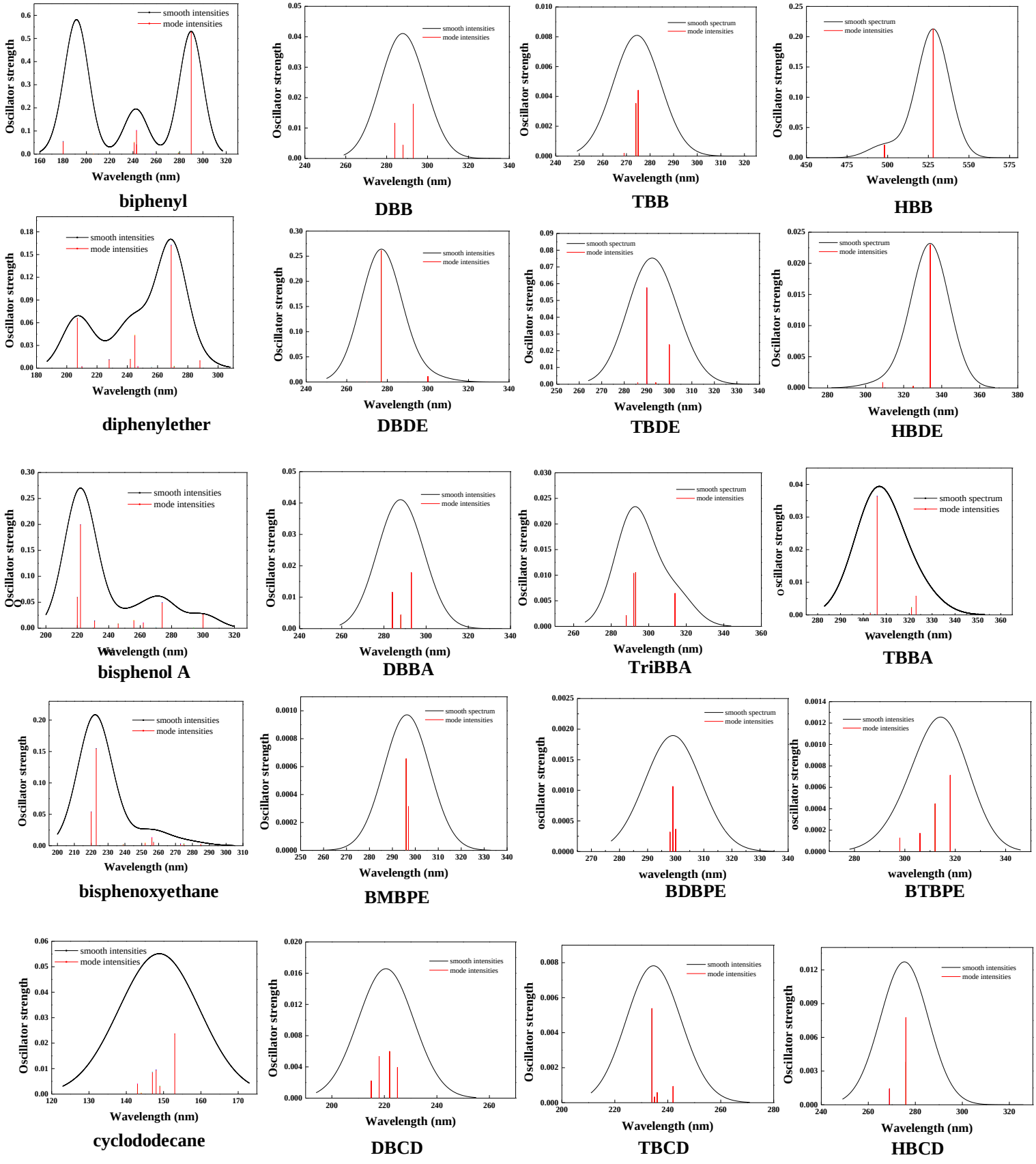

Fig. 6. The calculated gaseous-phase UV absorption spectra of studied BFRs and their non-brominated congeners.

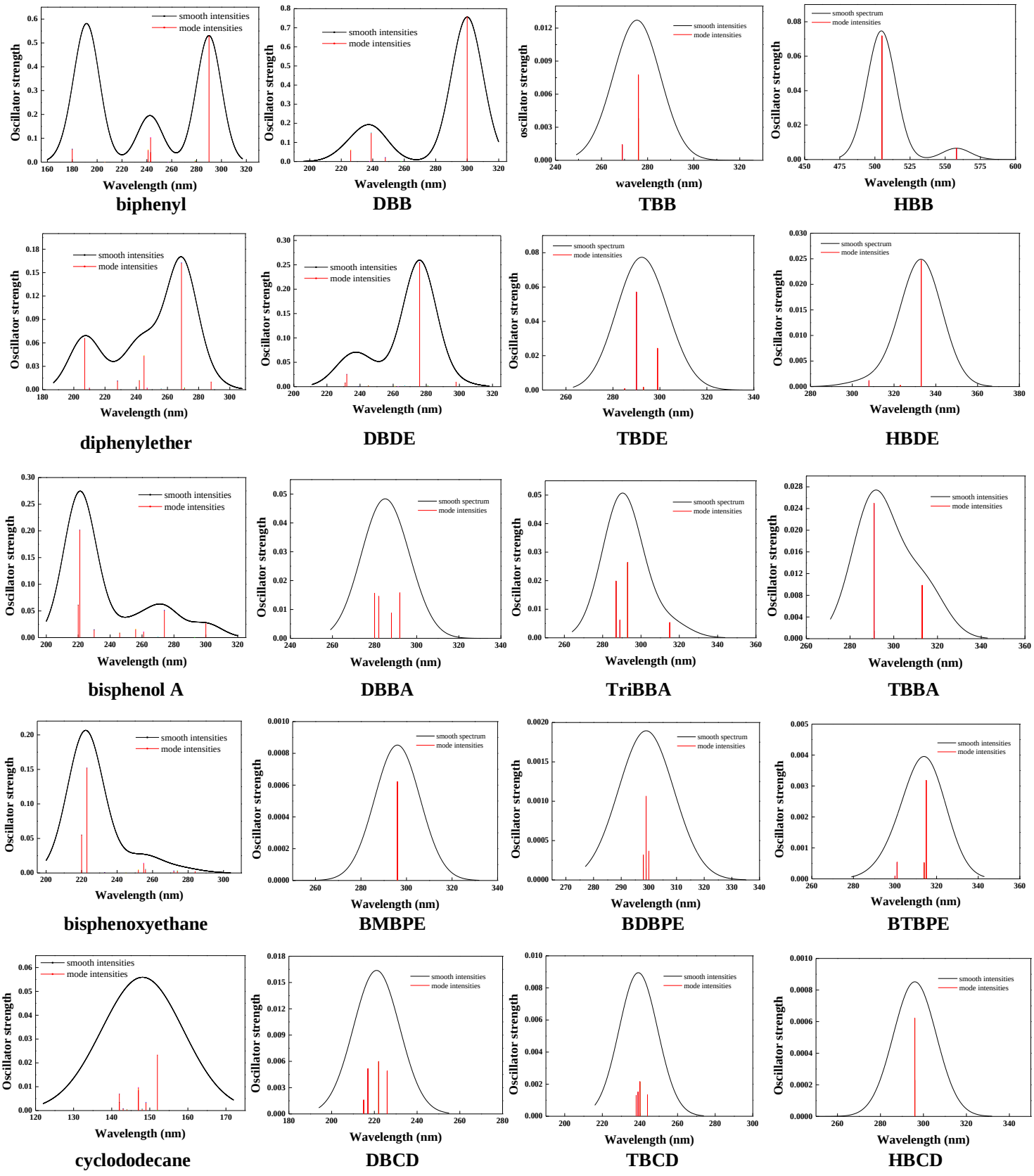

Fig. 7. The calculated aqueous-phase UV absorption spectra of studied BFRs and their non-brominated congeners.

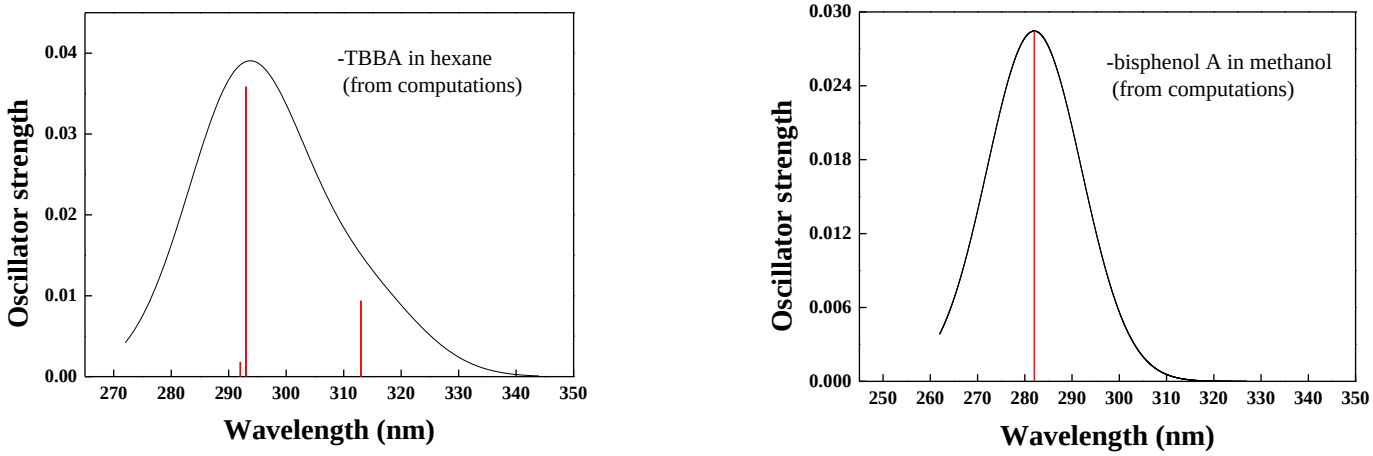

(a)

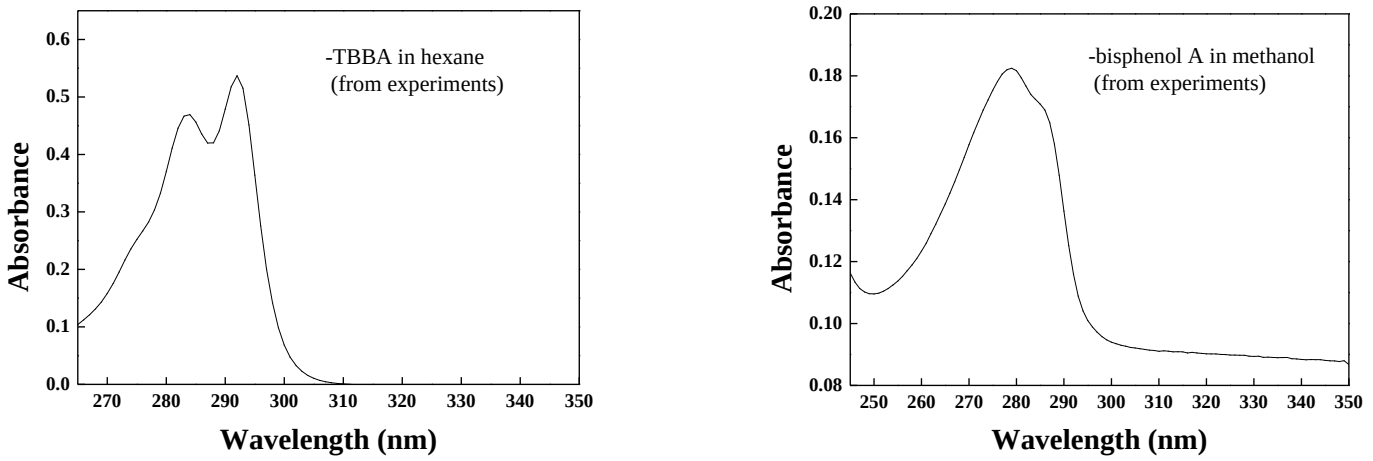

(b)

Fig. 8. UV-Vis spectra of TBBA and bisphenol A from (a) theoretical calculations and (b) experimental measurements in hexane and methanol, respectively.